

**CHAPTER 1 «PROPAGATION
OF THE TERAHERTZ LASER RADIATION
IN HOLLOW WAVEGUIDES»**

DOI: <https://doi.org/10.30525/978-9934-26-461-0-1>

Radiation beams formed in laser resonators and used for scientific and applied purposes usually have a Gaussian intensity distribution in their cross section. Oversized hollow metal and dielectric waveguides are used for constructing resonators and transmission lines in the terahertz frequency range. The designing of waveguide transmission lines requires information about energy losses in inhomogeneous radiation beams propagating in such systems, the conditions of their optimal excitation, the nature, magnitude and ways of minimising distortions introduced in the signals being transmitted.

The possibility of using waveguides with a diameter much larger than the wavelength as low-loss transmission lines was pointed out already in [49]. However, the problem of propagation of terahertz laser beams in waveguide systems has only recently been developed in a number of theoretical and experimental works. The data given in the literature refer to the transmission of radiation from gas discharge lasers in the form of individual waveguide modes and wave beams with a flat wavefront through hollow waveguides. However, radiation beams propagating in OPL (optically pumped lasers) resonators are formed due to the coherent summation of waveguide modes and have a close to Gaussian intensity distribution in the cross section with different levels of wavefront curvature.

In the THz range, the Marcatili-Schmeltzer ratio [50], which determines the excitation in waveguides of hybrid modes, is not satisfied for metal waveguides: $2\pi a / \lambda \gg |v| U_{mn}$, where a is the radius of the waveguide, v is the refractive index of the waveguide material, U_{mn} is the m -th root of the equation $J_{m-1}(U_{mn}) = 0$, integer subscripts m and n characterize the propagating hybrid mode. For this reason, the metal waveguide parameters are calculated by the mode technique using analytic expressions for the waveguide TE and TM modes obtained in the "ideal metal" approximation [51], although metals cannot be treated as ideal conductors in the short-wavelength part of the THz range. At the same time, dielectric waveguides are excited by strongly divergent radiation beams, when a considerable

part of the energy is transferred by higher modes, for which the Marcatili-Schmeltzer approximation may not be satisfied either. Therefore, a verification of the mode approach in these cases requires the use of an alternative (e.g., ray-optics) method. The ray-optics techniques being used at present [52, 53] need to be developed further since they do not take into account the interference of beams incident on and reflected from the waveguide walls.

In this chapter, we have studied theoretically and experimentally the transmission of OPL radiation with a Gaussian intensity profile through hollow metal and dielectric waveguides to determine the optimal conditions for waveguide excitation, minimum depolarisation of the initial beam, and to work out recommendations for using these waveguides in THz transmission lines.

1.1. PROPAGATION OF LASER RADIATION THROUGH HOLLOW CIRCULAR WAVEGUIDES

1.1.1. Mode and Ray-optics Methods of Calculation

1.1.1.1. Mode Approach for Dielectric Waveguides

This method can be used to analyze the transmission of radiation in both hollow circular dielectric and metallic waveguides. However, the main criterion for the excitation of hybrid modes in these waveguides is conformity to the Marcatili-Schmeltzer ratio [50]: $ka \gg |v|u_{mn}$, where a is the radius of the waveguide; v is the refractive index of the waveguide material; U_{mn} is the n th root of the equation $J_{m-1}(U_{mn}) = 0$ [J_{m-1} is the Bessel function of $(m - 1)$ -th order]. In the THz range, this ratio is not fulfilled for metal waveguides, therefore this method is used to analyze the propagation of radiation in hollow circular dielectric waveguides. Let's write the field configurations for the main modes of a hollow circular dielectric waveguide:

1. Circular electric modes TE_{0n} ($m = 0$)

$$E_{\phi 0n} = J_1(u_{0n}r) \cdot \exp(i\gamma_{0n}z - i\omega t),$$

$$H_{r0n} = -\sqrt{\frac{\epsilon_0}{\mu_0}} J_1(u_{0n}r) \cdot \exp(i\gamma_{0n}z - i\omega t),$$

$$H_{z0n} = -i\sqrt{\frac{\epsilon_0}{\mu_0}} \frac{u_{0n}}{ka} J_0(u_{0n}r) \cdot \exp(i\gamma_{0n}z - i\omega t).$$

2. Circular magnetic modes TM_{0n} ($m = 0$)

$$\begin{aligned} H_{\phi 0n} &= \sqrt{\frac{\varepsilon_0}{\mu_0}} J_1(u_{0n}r) \cdot \exp(i\gamma_{0n}z - i\omega t), \\ E_{r0n} &= J_1(u_{0n}r) \cdot \exp(i\gamma_{0n}z - i\omega t), \\ E_{z0n} &= i \frac{u_{0n}}{ka} J_0(u_{0n}r) \cdot \exp(i\gamma_{0n}z - i\omega t). \end{aligned}$$

3. Hybrid modes EH_{mn} ($m \neq 0$)

$$\begin{aligned} E_{\phi mn} &= \left[J_{m-1}(u_{mn}r) + \frac{i u_{mn}^2}{2nka} \sqrt{v^2 - 1} J'_m(u_{mn}r) \right] \cos m\phi \cdot \exp(i\gamma_{mn}z - i\omega t), \\ E_{r mn} &= \left[J_{m-1}(k_r r) + \frac{i u_{mn}}{2kr} \sqrt{v^2 - 1} J_m(u_{mn}r) \right] \sin m\phi \cdot \exp(i\gamma_{mn}z - i\omega t), \\ E_{z mn} &= -i \frac{u_{mn}}{ka} J_m(u_{mn}r) \sin m\phi \cdot \exp(i\gamma_{mn}z - i\omega t), \\ H_{\phi mn} &= \sqrt{\frac{\varepsilon_0}{\mu_0}} \left[J_{m-1}(u_{mn}r) + \frac{i u_{mn}}{2kr} \sqrt{v^2 - 1} J_m(u_{mn}r) \right] \sin m\phi \cdot \exp(i\gamma_{mn}z - i\omega t), \\ H_{r mn} &= -\sqrt{\frac{\varepsilon_0}{\mu_0}} \left[J_{m-1}(u_{mn}r) + \frac{i u_{mn}^2}{2nka} \sqrt{v^2 - 1} J'_m(u_{mn}r) \right] \cos m\phi \cdot \exp(i\gamma_{mn}z - i\omega t), \\ H_{z mn} &= i \sqrt{\frac{\varepsilon_0}{\mu_0}} \frac{u_{mn}}{ka} J_m(u_{mn}r) \cos m\phi \cdot \exp(i\gamma_{mn}z - i\omega t), \\ \gamma_{mn} &= \frac{2\pi}{\lambda} \left[1 - \frac{1}{2} \left(\frac{u_{mn}}{2\pi a} \right)^2 \left(1 - \frac{i v_{mn} \lambda}{\pi a} \right) \right], \\ v_{mn} &= \begin{cases} \frac{1}{\sqrt{v^2 - 1}} & \text{for } TE_{0n}, \\ \frac{v^2}{\sqrt{v^2 - 1}} & \text{for } TM_{0n}, \\ \frac{1 + v^2}{2\sqrt{v^2 - 1}} & \text{for } EH_{mn}. \end{cases} \end{aligned} \tag{1.1}$$

where r is the radial coordinate, ϕ is the polar angle, ω is the circular frequency of the wave, γ_{mn} are the propagation constants of the eigenmodes of the waveguide along the z axis:

Let's consider the excitation of a hollow circular dielectric waveguide by linearly polarized, for example, in the direction \vec{y} an axisymmetric Gaussian beam propagating along the axis of the waveguide. The beam waist is located at the entrance of the waveguide. For this beam the axis of symmetry coincides with the axis of the waveguide, and the radiation waist is located at the entrance of the waveguide. Then the initial radiation field in the cylindrical coordinate system has the form:

$$\vec{E}_{in}(\rho, \phi, 0) = E_0(\rho) \sin \phi \cdot \vec{\rho} + E_0(\rho) \cos \phi \cdot \vec{\phi}, \quad (1.2)$$

where $\vec{\rho}$, $\vec{\phi}$ are the unit vectors of polar coordinates,

$E_0(\rho) = E_0 \exp\left(-\frac{\rho^2}{w_0^2}\right)$, $w_0 = w'_0/a$, w'_0 is the radius of the beam waist in amplitude at the e^{-1} level from its maximum value.

For the polarisation of the initial radiation beam specified in this manner, only hybrid EH_{1n} modes described by orthonormal fields will propagate in the waveguide

$$\vec{V}_n(\rho, \phi, z) = V_0(\rho, z) \sin \phi \cdot \vec{\rho} + V_0(\rho, z) \cos \phi \cdot \vec{\phi}, \quad (1.3)$$

where $V_0(\rho, z) = \frac{\sqrt{2}}{\sqrt{\pi} \cdot J_1(u_{1n})} \cdot J_0(u_{1n}r) \cdot \exp(iz\gamma_{1n})$.

So, we can present the input radiation in the form of the following series

$$\vec{E}_{in}(\rho, \phi, 0) = \sum_{n=1}^M C_n \cdot \vec{V}_n(\rho, \phi, 0), \quad (1.4)$$

where $C_n = \int_0^{2\pi} \int_0^a \vec{E}_{in} \cdot \vec{V}_n \rho d\rho d\phi$ are the excitation coefficients of the corresponding hybrid modes, $M < \sqrt{\frac{a}{\lambda}}$ [54].

Then the field distribution \vec{E} and the beam power P_{out} in the waveguide cross-section at a distance L from its input end can be found from the expressions

$$\vec{E}(\rho, \phi, L) = \sum_{n=1}^M C_n \cdot \vec{V}_n(\rho, \phi, L), \quad (1.5)$$

$$P_{out}(L) = \sum_{n=1}^M |C_n|^2 \exp(-2\alpha_n L), \quad (1.6)$$

where $\alpha_n = \text{Im}(\gamma_{1n})$ are the attenuation coefficients of the corresponding waveguide modes.

The obtained relations allow us to determine the power transmission coefficient $T(L)$ of radiation in the waveguide and the degree of polarization of the output radiation $\Pi(L)$:

$$T(L) = P_{out}(L) / P_{in}, \quad \Pi(L) = \frac{I_y(L) - I_x(L)}{I_y(L) + I_x(L)}, \quad (1.7)$$

where $P_{in}(L) = \int_0^{2\pi} \int_0^\infty |\vec{E}(\rho, \phi, 0)|^2 \rho d\rho d\phi$ is the radiation power of the initial beam, $I_{x,y}(L) = \int_0^{2\pi} \int_0^a |E_{x,y}(\rho, \phi, L)|^2 \rho d\rho d\phi$.

1.1.1.2. Mode Approach for Metal Waveguides

This method is similar to the one described above. However, the calculation of the characteristics of circular oversized metal waveguide transmission lines is carried out using analytical expressions for waveguide TE and TM modes obtained in the approximation of an ideal metal [51].

Consider the excitation of a hollow circular metal waveguide by a linearly polarized Gaussian beam of the form (1.2). For the polarisation of the initial radiation beam specified in this manner, only the TE_{1n} and TM_{1n} waves will be excited in the waveguide. These modes are described by transverse orthonormal fields

$$\vec{V}_{1n}^{TE} = A_n \left[\frac{J_1(\nu_n r)}{r} \sin\phi \cdot \vec{\rho} + \frac{dJ_1(\nu_n r)}{dr} \cos\phi \cdot \vec{\phi} \right], \quad (1.8)$$

$$\vec{V}_{1n}^{TM} = B_n \left[\frac{dJ_1(\chi_n \rho)}{d\rho} \sin\phi \cdot \vec{\rho} + \frac{J_1(\chi_n \rho)}{\rho} \cos\phi \cdot \vec{\phi} \right], \quad (1.9)$$

where $A_n = \sqrt{\frac{2}{\pi}} \cdot \frac{1}{\sqrt{v_n^2 - 1}} \cdot \frac{1}{J_1(v_n)}$, $B_n = -\sqrt{\frac{2}{\pi}} \cdot \frac{1}{\chi_n} \cdot \frac{1}{J_2(\chi_n)}$, v_n is the n -th root of the equation $J_1'(v) = 0$, χ_n is the n -th root of the equation $J_1(\chi) = 0$.

Then the field distribution in the cross-section of the waveguide at a distance L from its input end has the form

$$\vec{E}(\rho, \phi, L) = \sum_n C_n \vec{V}_n^{TE} \exp(i\gamma_n^{TE} L) + \sum_n D_n \vec{V}_n^{TM} \exp(i\gamma_n^{TM} L), \quad (1.10)$$

where $C_n = \iint_0^{2\pi} \int_0^1 \vec{E}_{in} \cdot \vec{V}_n^{TE} \rho d\rho d\phi$, $D_n = \iint_0^{2\pi} \int_0^1 \vec{E}_{in} \cdot \vec{V}_n^{TM} \rho d\rho d\phi$ are the excitation coefficients of the corresponding modes, $\gamma_n = \beta_{1n} + i\alpha_{1n}$ are the propagation constants for the corresponding modes [51]:

$$\alpha_{1n}^{TE} = \frac{R_s}{R_0 \cdot a} \cdot \left[\frac{1}{v_n^2 - 1} + \left(\frac{\lambda}{\lambda_{1n}^{TE}} \right)^2 \right] \cdot \frac{1}{\sqrt{1 - \left(\frac{\lambda}{\lambda_{1n}^{TE}} \right)^2}},$$

$$\alpha_{1n}^{TM} = \frac{R_s}{R_0 \cdot a} \cdot \frac{1}{\sqrt{1 - \left(\frac{\lambda}{\lambda_{1n}^{TM}} \right)^2}},$$

$$\beta_{1n}^{TE, TM} = \frac{2\pi}{\lambda} \sqrt{1 - \left(\frac{\lambda}{\lambda_{1n}^{TE, TM}} \right)^2},$$

$\lambda_{1n}^{TE, TM}$ is the critical wavelength for TE and TM modes, $R_0 = 376.73 \Omega$ is the wave resistance of free space, R_s is the characteristic resistance of the metal walls of the waveguide.

Then the power of the beam at a distance L from the input end of the waveguide is equal

$$P_{out}(L) = \sum_n |C_n|^2 \exp(-2\alpha_n^{TE} L) + \sum_n |D_n|^2 \exp(-2\alpha_n^{TM} L). \quad (1.11)$$

The power transmission coefficient of the radiation in the waveguide and the degree of polarization of the output radiation are determined similarly by the expressions (1.7).

1.1.1.3 Frost's Geometrical Optics Approach

This method, described in [53], can be used to analyze the transmission of radiation in both hollow circular oversized dielectric and metallic waveguides. As will be shown below, the refractive index of the waveguide walls plays a significant role in the radiation propagation model.

Let a linearly polarized axially symmetric Gaussian beam with the polarization vector directed along the \vec{y} axis be incident on the entrance end of a circular waveguide ($z = 0$). The beam propagates along the \vec{z} axis of the waveguide in free space and the beam waist coincides with the input of the waveguide. Let's present the incident radiation in a general form in the Cartesian coordinate system

$$\vec{E}(\rho, 0) = E(\rho, 0) \cdot \vec{y}, \quad (1.12)$$

where

$$E(\rho, 0) = A_0 \exp\left[-\frac{\rho^2}{(w_0)^2}\right], \quad (1.13)$$

and ρ is the radial coordinate, w_0 is the beam radius measured at the e^{-1} level of its maximum amplitude at the waist; A_0 is the field amplitude of the beam.

We take into account the influence of the entrance aperture of the waveguide of radius a on the incident radiation and consider "weak" Gaussian beam diffraction. A Gaussian beam weakly diffracted by a circular aperture ($w_0 \leq 0.7a$) can be approximated in the far field by another Gaussian beam with slightly different characteristics [55]. The relationship between the parameters of the incident beam and the beam passing through the entrance aperture of the waveguide, is determined by the expressions:

$$w'_0 = w_0 \left[1 - \exp\left(-\frac{a^2}{w_0^2}\right) \right], \quad A'_0 = A_0 \left[1 - \exp\left(-\frac{2a^2}{w_0'^2}\right) \right] \left[1 - \exp\left(-\frac{a^2}{w_0'^2}\right) \right]^{-1} \quad (1.14)$$

where A'_0 is the field amplitude and w'_0 is the waist radius of the diffracted beam.

Considering the expression (1.14), radiation of the following form will be propagated in the waveguide:

$$\vec{E}'(\rho, z) = A'_0 \frac{w'_0}{w'(z)} \exp\left(-\frac{\rho^2}{2(w'(z))^2}\right) \cdot \exp\left\{i\left[\frac{2\pi}{\lambda}z - \arctg\left(\frac{\lambda z}{\pi w_0'^2}\right) + \frac{\rho^2 \pi}{\lambda R(z)}\right]\right\} \cdot \vec{y}, \quad (1.15)$$

where $w'(z) = w'_0 \sqrt{1 + \left(\frac{\lambda}{\pi(w'_0)^2}\right) z^2}$ is the radius of the beam, where the field decreases by a factor of e^{-1} , λ is the wavelength, $R(z) = z \left[1 + \left(\frac{\pi w_0'^2}{\lambda z}\right)^2\right]$ is the curvature radius of the wave front of the beam.

We decompose the field vector of the propagating beam into two components parallel and perpendicular to the plane of incidence on the waveguide wall:

$$\vec{E}'(\rho, \varphi, z) = \vec{\rho} E_{\parallel}(\rho, \varphi, z) + \vec{\varphi} E_{\perp}(\rho, \varphi, z), \quad (1.16)$$

where $E_{\parallel}(\rho, \varphi, z) = E'(\rho, z) \sin\varphi$, $E_{\perp}(\rho, \varphi, z) = E'(\rho, z) \cos\varphi$, $\vec{\rho}$, $\vec{\varphi}$, are the unit vectors of the cylindrical coordinates.

By using geometrical optics, we assume that a beam consists of ray tubes or rays contained in an elementary solid angle, lying in the meridional planes of the waveguide and having a common origin – the center of the beam. In such an analysis, it is not possible to determine the field at the axis of the waveguide [56]. At any other point of observation in the waveguide, the field is a superposition of the fields of the incident ray and the ray reflected from the waveguide wall. These rays can be assumed to emerge from the points displaced by $2an$ along ρ (Figure 1.1), where n is the number of reflections from the wall:

$$E_{\parallel, \perp}(\rho, \varphi, z) = \sum_{n=-N}^N E'_n(\rho_n, z) r_{\parallel, \perp}^{|n|} \begin{Bmatrix} \sin\varphi \\ \cos\varphi \end{Bmatrix}, \quad (1.17)$$

where $\rho_n = 2an + (-1)^n \rho$, r_{\parallel}, r_{\perp} are Fresnel's reflection coefficients [9]. They have the following form

$$r_{\parallel} = \frac{[n_2^2(1-k_2^2) + 2in_2^2k_2] \cos\Theta_m - n_1(u_2 + iv_2)}{[n_2^2(1-k_2^2) + 2in_2^2k_2] \cos\Theta_m + n_1(u_2 + iv_2)}, \quad r_{\perp} = \frac{n_1 \cos\Theta_m - (u_2 + iv_2)}{n_1 \cos\Theta_m + (u_2 + iv_2)}, \quad (1.18)$$

where n_1 is the refraction index of the medium in the waveguide, n_2, k_2 are determined from the expression for the refractive index of the waveguide wall $\hat{n}_2 = n_2(1 + ik_2)$, u_2, v_2 , according to the ratio $\hat{n}_2 \cos\Theta_m = u_2 + iv_2$, Θ_m, Θ_m

are the angles of incidence and refraction of the beam. The angle of incidence is determined by expressions

$$\Theta_{in} = \frac{\pi}{2} - |\Theta_n|, \quad \Theta_n = \arctg\left(\frac{\rho_n}{z}\right). \quad (1.19)$$

The cross-sectional area of the ray tube, which it would have possessed in the absence of reflections (Figure 1.2), is equal to $dS_n = \zeta_n^2 \sin \Theta_n d\varphi d\Theta_n$, where $\zeta_n = \frac{z}{\cos \Theta_n}$ is the distance to the observation point along the beam.

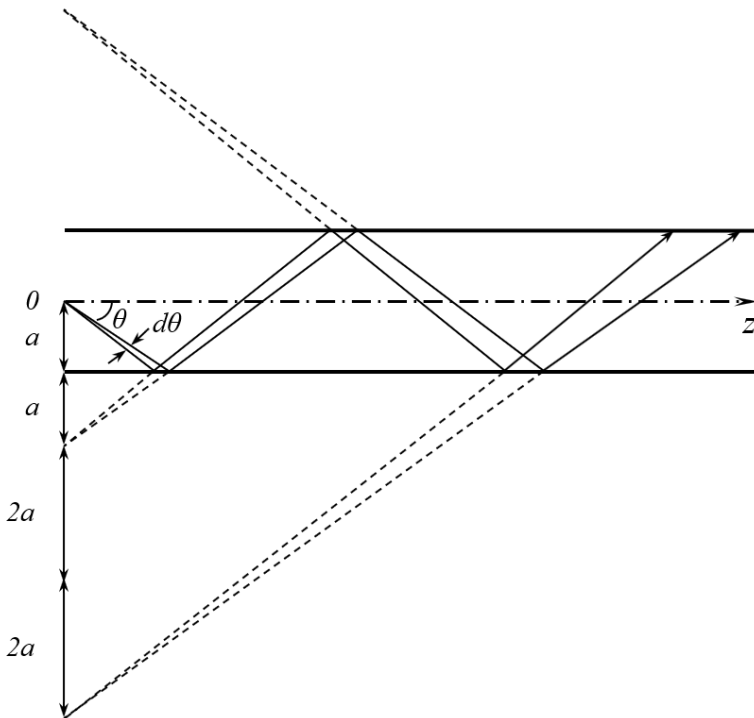


Figure 1.1. Schematic representation of the decomposition of the input beam into elementary ray tubes and their transmission along the waveguide

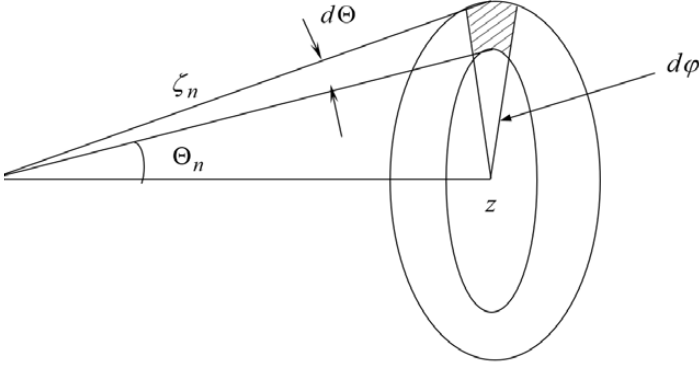


Figure 1.2. Cross section of beam tube

Then the energy flux passing through this cross section is:

$$dW = I'(\rho_n, z) z^2 \frac{\text{tg } \Theta}{\cos \Theta_n} d\varphi d\Theta_n,$$

where $I'(\rho_n, z) = |E'(\rho_n, z)|^2$ is the intensity of radiation in a cross-section perpendicular to the beam.

We assume that a ray tube after reflection is focused into a line along the waveguide axis. In this case, the cross-sectional area of the ray tube at the point of observation is

$$dS = \zeta \sin \Theta d\varphi \zeta_n d\Theta = z \frac{2 \text{tg } \Theta}{\cos \Theta_n} d\varphi d\Theta,$$

where $\zeta = \frac{z}{\cos \Theta}$; $\Theta = \text{arctg} \left(\frac{\rho \lambda}{\pi \omega_0^2 a z} \right)$ is the angle at which this point is seen from center of the beam.

Because the energy flux in a ray tube is constant, the intensity $I'_n(\rho, z)$ at the given point is related to the intensity $I'(\rho_n, z)$ in the unfocused beam by the expression

$$I'_n(\rho, z) = \frac{dW}{dS} = I'(\rho_n, z) \left| \frac{\rho_n}{\rho} \right|,$$

while the intensity of the rays in the cross-section perpendicular to the waveguide axis is equal $I_n(\rho, z) = I'_n(\rho, z) \cos \Theta_n$. Thus, the field of the n th ray in (2.17) has the form

$$E'_n(\rho_n, z) = E'(\rho, z) \sqrt{\left| \frac{\rho_n}{\rho} \right|} \cos \Theta_n. \quad (1.20)$$

Thus, the total intensity at any point of the waveguide will be determined by the following expression

$$I(\rho, \varphi, z) = I_{\parallel}(\rho, \varphi, z) + I_{\perp}(\rho, \varphi, z), \quad (1.21)$$

where

$$I_{\parallel}(\rho, \varphi, z) = \sum_{n=-N}^N \left| E'(\rho_n, z) \sqrt{\left| \frac{\rho_n}{\rho} \right|} \cos \Theta_n r_n^{|\mu|} \sin \varphi \right|^2,$$

$$I_{\perp}(\rho, \varphi, z) = \sum_{n=-N}^N \left| E'(\rho_n, z) \sqrt{\left| \frac{\rho_n}{\rho} \right|} \cos \Theta_n r_n^{|\mu|} \cos \varphi \right|^2.$$

The power of the beam at a distance L from its entrance end

$$P_{out}(L) = \int_0^{2\pi} \int_0^a I(\rho, \varphi, L) \rho d\rho d\varphi. \quad (1.22)$$

The power transmission coefficient of radiation in the waveguide and the degree of polarization of the output radiation are determined by expressions (1.7).

However, this approach has limitations on the length of the waveguide, so the length of the waveguide should not exceed the value a^2/λ [56]. This is due to the fact that complex interference effects arise in the waveguide between the incident and reflected beams, which this approach does not take into account.

1.1.1.4. Crenn's Geometrical Optics Approach

Using the ray-optics representation, we assume that the incident beam consists of elementary beams with a power of dP , contained in an elementary solid angle, lying in the meridional planes of the waveguide and having a common origin – the center of the beam [52]. At the waveguide input, the power of the elementary beam has the following form

$$dP = I(\rho_0, 0) \rho_0 d\rho_0 d\varphi = I_0 \exp\left(-\frac{\rho_0^2}{w_0^2}\right) \rho_0 d\rho_0 d\varphi, \quad (1.23)$$

where ρ_0 is the radial coordinate, φ is the polar angle in the transverse plane (Figure 1.3), I_0 is the beam intensity on the axis at the waveguide entrance, w_0 is the beam radius at the waveguide entrance.

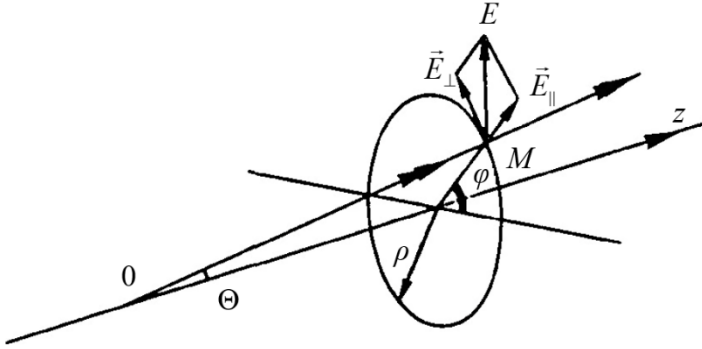


**Figure 1.3. Electric field at point M.
The plane of the circle is perpendicular to the z axis**

The reflection coefficients on the wall depend on the complex refractive index \bar{v} of the wall material given by

$$\bar{v} = v \exp(i\varphi) = \sqrt{\varepsilon - i \frac{\sigma}{\varepsilon_0 \omega}}$$

For metallic waveguides made of copper, silver, gold, or brass, the conductivity σ is larger than $10^7 \Omega^{-1}/\text{m}$. At IR frequencies, the corresponding values of the refractive index of the waveguide material v are several hundreds. Consequently, the values of v are very large, and despite the paraxial approximation the condition $\Theta v \ll 1$ is not always true for the Gaussian beams. Thus, the term Θv cannot be neglected in the calculations. Therefore, as a condition for the paraxial approximation

$$\text{tg}\Theta \approx \Theta, \Theta = \frac{\rho_0}{k\omega_0^2} \ll 1, \tag{1.24}$$

and the condition $v \gg 1$ must be taken into account in these calculations. Due to these large values of v , one has

$$\frac{\sigma}{\varepsilon_0 \omega} \gg \varepsilon, \quad \bar{v} = (1 - i) \sqrt{\frac{\sigma}{2\varepsilon\omega}}$$

Assuming the paraxial approximation, i.e., the angle Θ is small, and using a first-order expansion in Θ , the following approximate relations can

be derived for angles of incidence Θ_{in} and reflection Θ_m of radiation on the waveguide wall

$$\begin{aligned}\sin\Theta_{in} &= \cos\Theta \approx 1, \\ \sin\Theta_m &\approx \frac{1}{\bar{v}}, \\ \cos\Theta_{in} &= \sin\Theta \approx \Theta, \\ \cos\Theta_m &\approx \sqrt{1 - \left(\frac{1}{\bar{v}}\right)^2}.\end{aligned}\tag{1.25}$$

Using Eqs. (1.18) and (1.25) and a first-order expansion in Θ and $(1/\bar{v})^2$, we find for the reflection coefficients

$$\bar{r}_\perp = -1 + \frac{2\Theta}{\bar{v}},\tag{1.26}$$

$$\bar{r}_\parallel = 1 - \frac{2\Theta\bar{v}}{1 + \Theta\bar{v}}.\tag{1.27}$$

From Eqs. (1.26) i (1.27) one obtains

$$r_\perp^2 = 1 - \frac{2\sqrt{2}\Theta}{\bar{v}},\tag{1.28}$$

$$r_\parallel^2 = 1 - \frac{2\sqrt{2}\Theta\bar{v}}{1 + \sqrt{2}\Theta\bar{v} + \Theta^2\bar{v}^2},\tag{1.29}$$

where r_\parallel and r_\perp are, respectively, the moduli of \bar{r}_\parallel and \bar{r}_\perp .

The intensity of the incident beam is related to the electric field by (Fig. 1.3)

$$I \approx E^2 = E_\parallel^2 + E_\perp^2 = E^2 \sin^2\varphi + E^2 \cos^2\varphi.\tag{1.30}$$

The intensity of the reflected beam is expressed as

$$r^2(\Theta, \varphi)I = (r_\parallel^2 \sin^2\varphi + r_\perp^2 \cos^2\varphi)I.\tag{1.31}$$

This intensity is the sum of two components, corresponding to E_\parallel and E_\perp . Because Θ and $1/\bar{v}$ are small, Eqs. (1.28) and (1.29) show that the coefficient r_\perp is very close to unity, but this is not always true for r_\parallel . Therefore, after one reflection, a strong depolarization of the beam may occur, and it cannot be assumed that the incident Gaussian beam will retain

its polarization inside the waveguide. The experimental results in [57] agree well with this statement. After n reflections in the waveguide, the output intensity of the components E_{\parallel} and E_{\perp} is proportional, respectively, to r_{\parallel}^{2n} and r_{\perp}^{2n} . Note that the number of reflections n depends on the angle Θ or on ρ_0 (Eq. 2.24).

Consider an elementary ring in the cross section of a Gaussian beam, defined by $(\rho_0, d\rho_0)$. After n reflections in the waveguide, the beam power in this ring is calculated from the expression

$$\begin{aligned} I'_0 \exp\left(-\frac{\rho_0^2}{w_0'^2}\right) \rho_0 d\rho_0 d\varphi \int_0^{2\pi} \left[r_{\parallel}^{2n(\rho_0)} \sin^2\varphi + r_{\perp}^{2n(\rho_0)} \cos^2\varphi \right] d\varphi = \\ = 2\pi I'_0 t_n \exp\left(-\frac{\rho_0^2}{w_0'^2}\right) \rho_0 d\rho_0, \end{aligned} \quad (1.32)$$

where w_0' and I'_0 are determined, respectively, from (Eq. 1.14) and the transmission coefficient $t_n(\rho_0)$ is found as

$$t_n(\rho_0) = \frac{r_{\parallel}^{2n(\rho_0)} + r_{\perp}^{2n(\rho_0)}}{2}. \quad (1.33)$$

Accordingly, using expression (1.32), the power $P_{out}(L)$ can be calculated as

$$P_{out}(L) = 2\pi I'_0 \int_0^{\rho_m} t_n(\rho_0) \exp\left(-\frac{\rho_0^2}{w_0'^2}\right) \rho_0 d\rho_0. \quad (1.34)$$

The coefficient $t_n(\rho_0)$ depends on the function $n(\rho_0)$, which, when it is approximated by a linear function using (Eq. 1.24), has the form:

$$n = \frac{L\Theta}{2a} = \frac{L\rho_0}{2akw_0'^2}. \quad (1.35)$$

Equation (1.35) allows us to calculate the coefficients $r_{\perp}^{2n(\rho_0)}$, $r_{\parallel}^{2n(\rho_0)}$ and $t_n(\rho_0)$.

1. Calculation $r_{\perp}^{2n(\rho_0)}$. Since the coefficient r_{\perp}^2 determined from (1.28) is very close to 1 ($\Theta \ll 1$ and $v \gg 1$), the following exponential approximation is made to simplify the calculation of the integral (1.34):

$$r_{\perp}^2 = \exp\left(-\frac{2\sqrt{2}\Theta}{v}\right). \quad (1.36)$$

Then the coefficient $r_{\perp}^{2n(\rho_0)}$ is derived from Eqs. (1.24), (1.35) and (1.36) as

$$r_{\perp}^{2n} = \exp\left(-\frac{\sqrt{2} L}{v} \frac{\rho_0^2}{a k^2 w_0'^4}\right). \quad (1.37)$$

2. Calculation $r_{\parallel}^{2n(\rho_0)}$. The expression for the coefficient r_{\parallel} defined by Eq. (1.29) does not lead to a simple calculation of the integral (1.34). So, in the considered range of incidence angles, the function given by Eq. (1.29) is well approximated by the exponential function

$$3. \quad \begin{aligned} r_{\parallel}^2 &= \exp[-(1 + \sqrt{2})\Theta v] \text{ for } 0 \leq \Theta v \leq 1, \\ r_{\parallel}^2 &= \exp\left(-\frac{1 + \sqrt{2}}{\Theta v}\right) \text{ for } \Theta v > 1. \end{aligned} \quad (1.38)$$

Then the coefficient r_{\parallel}^{2n} is derived from Eqs. (2.24), (2.35) and (2.38):

$$\begin{aligned} r_{\parallel}^{2n} &= \exp\left[-\frac{(1 + \sqrt{2})v L}{2} \frac{\rho_0^2}{a k^2 w_0'^4}\right] \text{ for } 0 \leq \rho_0 \leq \frac{k w_0'^2}{v}, \\ r_{\parallel}^{2n} &= \exp\left[-\frac{(1 + \sqrt{2})v L}{2v} \frac{\rho_0^2}{a}\right] \text{ for } \rho_0 > \frac{k w_0'^2}{v}. \end{aligned} \quad (1.39)$$

To simplify the writing of formulas, we denote

$$F_1 = 1 + \frac{\sqrt{2} L}{v} \frac{1}{a k^2 w_0'^2}, \quad 1 + \frac{(1 + \sqrt{2})v L}{2} \frac{1}{a k^2 w_0'^2}. \quad (1.40)$$

Substituting values of Eqs. (1.33), (1.37), (1.39) and (1.40) into (1.34), the output power $P_{out}(L)$ is defined as

$$\begin{aligned} P_{out}(L) &= \pi I_0' \int_0^{\rho_m} \exp(-F_1 \frac{\rho_0^2}{w_0'^2}) \rho_0 d\rho_0 + \pi I_0' \int_0^{k w_0'^2/v} \exp(-F_2 \frac{\rho_0^2}{w_0'^2}) \rho_0 d\rho_0 + \\ &+ \pi I_0' \exp\left(-\frac{1 + \sqrt{2} L}{2v} \frac{1}{a}\right) \int_{k w_0'^2/v}^{\rho_m} \exp\left(-\frac{\rho_0^2}{w_0'^2}\right) \rho_0 d\rho_0. \end{aligned} \quad (1.41)$$

Integration of Eq. (1.41) yields the result

$$P_{out}(L) = \frac{\pi I'_0 w_0'^2}{2F_1} \left[1 - \exp\left(-F_1 \frac{\rho_m^2}{w_0'^2}\right) \right] + \frac{\pi I'_0 w_0'^2}{2F_2} \left[1 - \exp\left(-F_2 \frac{k^2 w_0'^2}{v^2}\right) \right] + \frac{\pi I'_0 w_0'^2}{2} \exp\left(-\frac{1 + \sqrt{2}}{2v} \frac{L}{a}\right) \left[\exp\left(-\frac{k^2 w_0'^2}{v^2}\right) - \exp\left(-\frac{\rho_m^2}{w_0'^2}\right) \right]. \quad (1.42)$$

From Eq. (1.40), taking into account (1.24), we find that

$$\exp\left(-F_1 \frac{\rho_m^2}{w_0'^2}\right) \approx 0. \quad (1.43)$$

Then, considering that the power of the diffracted Gaussian beam is equal to

$$P' = \pi I'_0 w_0'^2 = P \left[1 - \exp\left(-\frac{a^2}{w_0'^2}\right) \right], \quad (1.44)$$

Where w_0' is given by Eq. (1.14) and using Eqs. (1.24), (1.42–1.44) we will obtain an expression for calculating the transmission coefficient of a Gaussian beam in a waveguide with high conductivity of the wall material:

$$T = \frac{1 - \exp\left(-\frac{a^2}{w_0'^2}\right)}{2} \left[\frac{1}{F_1} + \frac{1}{F_2} + \left(1 - \frac{1}{F_2}\right) \exp\left(-F_2 \frac{k^2 w_0'^2}{v^2}\right) \right]. \quad (1.45)$$

1.1.2. Conditions of Application of Geometrical Optics Approaches in Oversized Metal Waveguides

Using the methods described above, calculations were performed for the transmission coefficient and the degree of polarization of the field in circular copper waveguides excited by linearly polarized Gaussian beams of THz radiation with a field of type (1.12). The radiation frequency was varied from 4 to 28 THz. The studies were performed when the relative radius of the output beam was changed in the range from 0.1 to 0.7 (in the region of its "weak" diffraction [55]). For copper the surface resistance was $R_s = 2.625 \times 10^{-7} (c/\lambda)^{1/2}$, taking into account the specific conductivity of the metal at direct current $\sigma_0 = 5.73 \times 10^7$ S/m [58]. The refractive index of copper for the corresponding radiation frequency was chosen according to [59].

Figure 1.4 shows the results of calculations of the transmission characteristics of the copper waveguide with a diameter $2a = 3$ mm and length $L = 370$ mm using the Crenn's geometrical optics approach (subchapter 1.1.1.4) and the mode approaches in the approximations of a real metal both by an "ideal metal" and a dielectric. As a reference graph of the radiation transmission coefficient in the frequency range from 4 THz to 28 THz, we selected the curve calculated using ray-optics theory, because its calculation is not related to the existence of a certain set of waveguide modes, and only depends on the refractive index of the waveguide material at a given frequency.

We can distinguish three regions of the terahertz range, where the results obtained using the mode approach in calculating the transmission characteristics of metallic waveguides are different. In the frequency range above 15 THz ($\lambda < 20$ μm), the mode approach in approximation the real metal by a dielectric gives more reliable results (Figure 1.4a). At frequencies below 7.5 THz ($\lambda \geq 40$ μm), there is a better agreement between the results of calculations with the help of the ray-optics and mode method in the approximation of an ideal metal (Figure 1.4d, e, f). In the frequency range from 7.5 to 15 THz (20 $\mu\text{m} \leq \lambda < 40$ μm), the choice of the calculation method is determined by the relative radius of the exciting beam w_0 (Figure 1.4b, c).

When $w_0 < 0.3$, the application of the mode technique in the approximation of an ideal metal gives the best results, and when $w_0 > 0.3$ – in the approximation of a metal by a dielectric. This can be explained by an increase in the refractive index of copper with a decrease in the frequency of transmitted radiation. At a radiation frequency below 7.5 THz, copper in its electrodynamic properties is close to an ideal metal (Figure 1.5).

Measurements were made of the transmission coefficient and the degree of polarization of radiation in a copper waveguide with a diameter of 3 mm and a length of 370 mm when it was excited by linearly polarized beams of a Gaussian intensity profile of the type (1.12) from an optically pumped CH_3OH laser ($f = 4.25$ THz, $\lambda = 70.5$ μm) and a stabilized CO_2 laser ($f = 28.3$ THz, $\lambda = 10.6$ μm). In calculating the transmission coefficient of the waveguide, radiation attenuation in the atmosphere inside the waveguide was taken into account. At various days during the experimental studies, it varied in the range 3–3.4 dB m^{-1} depending on the air humidity in

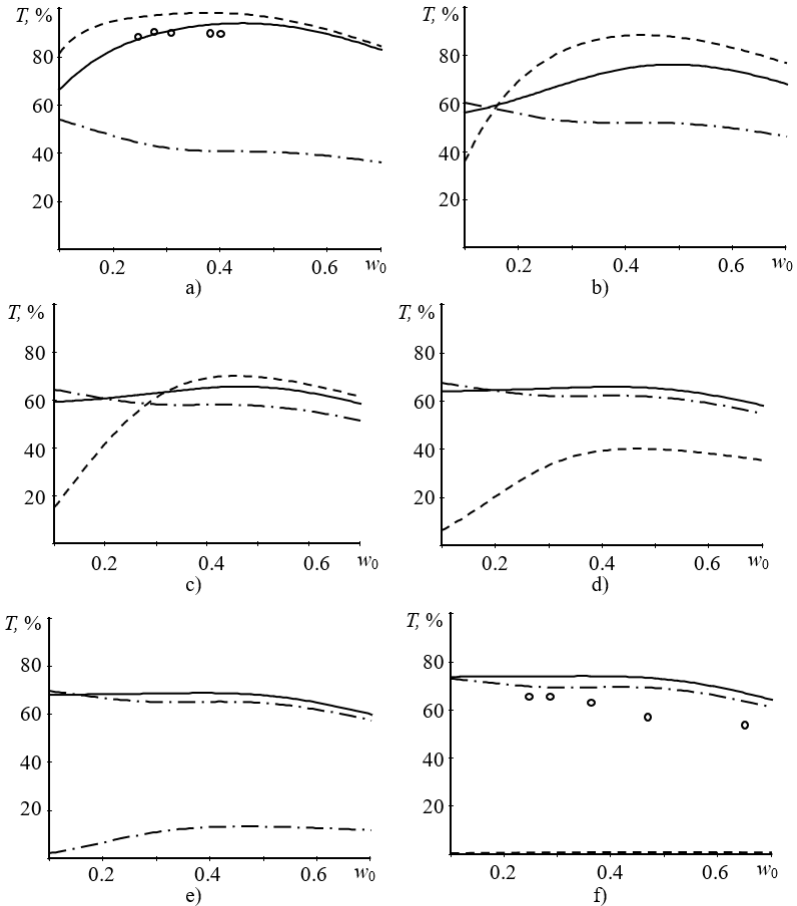


Figure 1.4. Calculated (curves) and experimental (points) dependences of the radiation transmission coefficient T on the relative radius w_0 of the exciting beam in the copper waveguide at $2a = 3$ mm, $L = 370$ mm.

Solid curves – calculation using the geometric-optical method, dashed – using the mode method in the approximation of a metal with a dielectric, dash-dotted – using the mode method in the approximation of an ideal metal. a) $f = 28.3$ THz, b) 15 THz, c) 10 THz, d) 7.5 THz, e) 6 THz, f) 4.25 THz

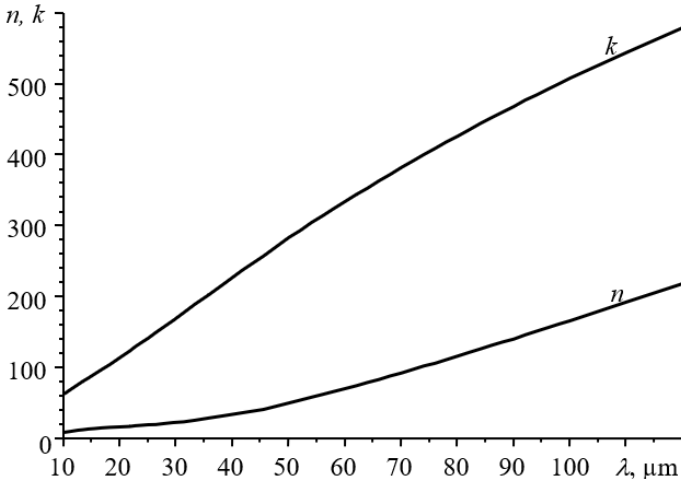


Figure 1.5. Dependence of the calculated refractive index of copper $n^* = n + ik$ on the wavelength λ of radiation propagating along a circular metal waveguide

the laboratory. Experimental points in the dependence of the transmission coefficient on the relative radius of the exciting beam w_0 for the given frequency are presented in Figure 1.4e.

There is a good agreement between the experimental and calculated data obtained using the mode approach in the approximation of an ideal metal. At the same time, depolarization of the laser radiation that passed through the waveguide was observed. The measured degree of its polarization at different w_0 varied from 10 % to 50 %. This indicates that in a metallic waveguide excited by a linearly polarised Gaussian beam at a given frequency, TE_{1n} and TM_{1n} waves with the field polarisation differing from linear one are excited.

When measuring the transmission characteristics at the frequency $f = 28.3$ THz ($\lambda = 10.6 \mu\text{m}$) a stabilised LG-74 CO_2 laser was used as a radiation source. Formation of Gaussian beams with a flat phase front was carried out using NaCl lenses with different focal lengths. The results of the experiment are shown in Fig. 1.4 a. There is a good agreement between the experimental results and calculations based on the mode method

using the approximation of the metal by a dielectric at this frequency. It is known that hybrid EH_{1m} modes have linear polarization. The measured degree of polarization of the radiation that passed through the investigated waveguide, in the case of its excitation by a linearly polarized beam with a relative radius $w_0 = 0.5$, was equal to $\Pi = 99.3\%$. For a similar segment of the dielectric waveguide the measured degree of polarization of the output radiation is $\Pi = 99.8\%$ for the same parameters of the exciting beam. This experiment allows us to assert that in the investigated copper waveguide EH_{1m} hybrid modes are excited at a given frequency.

The discrepancy between the calculated and experimental data is explained by the irregular cross section, surface roughness and possible difference in the calculated material constants for the waveguides used in the study.

For quantitative evaluation of the appropriateness of the mode approach in the terahertz range, we calculated the dependence of the normalised average absolute deviation Δ of the transmission coefficients on the relative beam radius w_0 , found using the ray-optics (G) and mode (R) approaches [60]:

$$\Delta(w_0) = |G(w_0) - R(w_0)|.$$

Figure 1.6 shows the calculated dependences of the difference measure Δ of the transmission coefficient on the radiation frequency f (wavelength λ) and the relative radius w_0 of the exciting beam in the copper waveguide at $2a = 3$ mm, $L = 370$ mm.

Calculations were performed using the ray-optics and mode methods in the approximation of the metal by a dielectric (Figure 1.6a), as well as using ray-optics and mode methods in the ideal-metal approximation (Figure 1.6b). These results confirm the presence of a transition region in the behavior of the electrodynamic properties of metal waveguides in the frequency range of 7.5 – 15 THz. In this frequency range, the determining parameter for assessing the applicability of mode approaches is the value of the relative radius of the radiation beam.

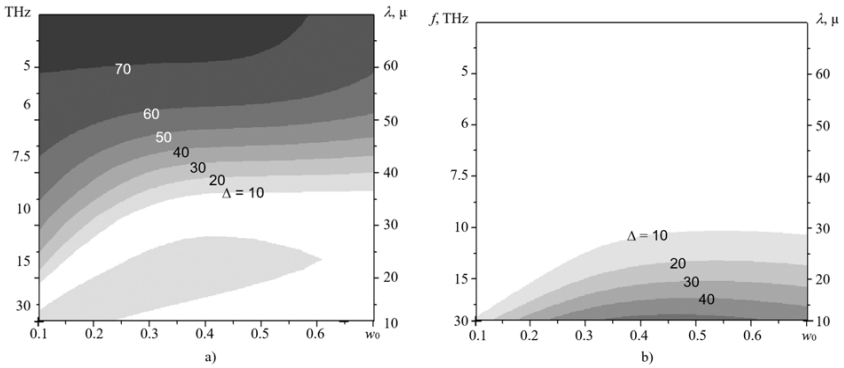


Figure 1.6. Calculated dependences of the deviation Δ of the transmission coefficient on the radiation frequency f (wavelength λ) and the relative radius w_0 of an exciting beam in a copper waveguide

1.1.3. Attenuation of EH_{11} Type Oscillations in Dielectric Waveguides

Attenuation in waveguides is one of the most important characteristics determining the choice of their geometric dimensions. The attenuation in glass and quartz waveguides was calculated and measured at two THz wavelengths, 337 μm and 118.8 μm , both for the single-mode EH_{11} regime achieved by self-filtering or direct excitation, and for a multimode signal. In the latter case, excitation was performed by a laser with a central hole in the output reflector.

The EH_{11} mode is linearly polarized, its field intensity maximum is on the axis, its phase front is nearly planar, and it is excited efficiently by the fundamental oscillation mode in laser resonators [61]. This causes interest in its real characteristics when the radiation is transmitted through a waveguide, first of all, in the attenuation constant α_{11} . Its analytical expression was obtained in [50] and has the following form:

$$\alpha_{11} = \left(\frac{U_{01}}{2\pi} \right)^2 \frac{\lambda^2}{a^3} \text{Re}(v_{EH}). \quad (1.46)$$

Difficulties in determining α_{11} according to (1.46) are associated with the absence of data on the parameters of the materials from which hollow dielectric waveguides are made in the THz range. Conducting experimental

studies makes it possible to overcoming these difficulties. The block diagram of the experimental setup is shown in Figure 1.7. A laser emitting on CH_3OH ($\lambda = 118.8 \mu\text{m}$) [62] and HCN ($\lambda = 337 \mu\text{m}$) [63] molecules served as a radiation source (1). The HCN laser is excited by a separate HF generator at a frequency of 13.56 MHz. The laser emits the EH_{11} fundamental mode with a linear ($\sim 100\%$) polarization. Its resonator is formed by a glass tube 2.3 m long and with an inner diameter of $2a = 56 \text{ mm}$ and two flat mirrors, one of which contains a coupling hole ($d = 8 \text{ mm}$). In the process of research, a one-dimensional wire grating with a step of $40 \mu\text{m}$ and a wire diameter of $8 \mu\text{m}$ was also used as an output element. The output power of the radiation was at least 60 mW.

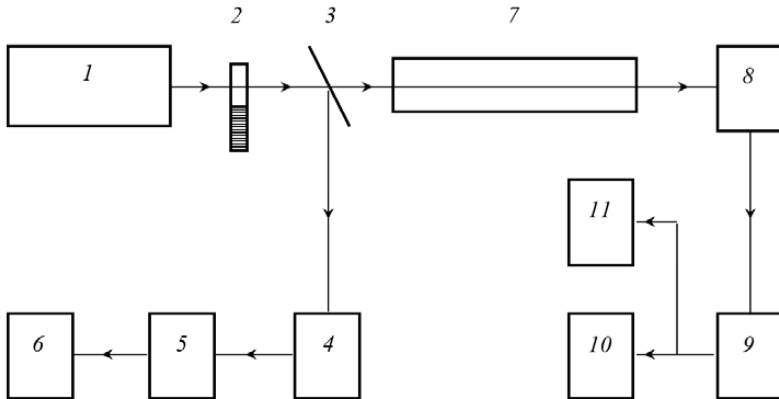


Figure 1.7. Structural diagram of the experimental equipment:
(1) THz laser; (2) modulator; (3) divider of THz radiation;
(4, 8) pyroelectric receivers; (5, 9) measuring amplifiers;
(6, 10) oscilloscopes; (7) waveguide under study; (11) recorder

The radiation is modulated in amplitude by a mechanical chopper (2) with a frequency of 30 Hz at the output of the laser. Part of the radiation ($\sim 10\%$) is diverted using a beam splitter (3) to control the output power of the laser. The main part of the radiation is used to study hollow dielectric waveguides (7). At the output of the studied waveguide, the radiation arrives at pyroelectric receiver (8), insensitive to the polarization of the radiation incident on it. From the output of the receiver, the electrical signal

is fed to the selective amplifier B6-4, tuned to the modulation frequency. The amplified signal is detected and registered using a recorder (11). Oscilloscopes (6, 10) are used for visual observation of the signal from the output of the selective amplifier.

Measurement of the spatial distribution of the intensity of the EH_{11} mode emitted by the laser at various distances from the laser and the waveguide is performed by scanning the receiver (8) across the beam both in the vertical and horizontal planes. The distance from the exit window can vary within a wide range from 0.15 m to 3 m. At any point it is possible to register the radial profile of laser radiation. Binding to the center of the laser aperture along the entire length of the path is carried out using a He-Ne laser. The pyroelectric detector made of $LiNbO_3$ crystal serves as a laser radiation signal receiver. Like all thermal receivers, it does not have selective properties and its frequency response is determined only by the properties of the absorbing layer. The pyroelectric current is directly proportional to the absorbed power and depends on the thermal characteristics of the sample. The threshold sensitivity of the pyroelectric receiver is not worse than 10^{-8} W/Hz. Bolometric receiver with a measurement error of $\sim 10\%$ was used to measure the absolute value of the laser output power, as well as to estimate the attenuation in the waveguide.

Measurements of α_{11} were performed by indirect and direct methods. The indirect method was based on a comparison of the losses of the TEM_{00} mode of an open cavity with the losses of the EH_{11} mode of a resonant system of a waveguide laser having the same mirrors. An HCN laser with a wavelength of $337 \mu\text{m}$ served as the signal source. Its open resonator had a semiconfocal geometry with mirrors characterized by the radii of curvature $R_1 = 3, 4, \text{ and } 5 \text{ m}$, and $R_2 = \infty$; the diameters of the mirror apertures were 60, 80, and 100 mm, respectively. In these configurations the diffraction losses were much less than the sum of the coupling losses and those due to heating of the mirrors. The losses experienced by the EH_{11} mode could then be higher than those in the case of the TEM_{00} mode by an amount governed by the attenuation in the walls and in the medium (in the case of resonators of different lengths). The measured attenuations for the EH_{11} mode in waveguide laser tubes with diameters 36, 56, and 80 mm were found to be 0.012, 0.0035, and 0.0011 m^{-1} , respectively. The results of

these measurements led to a scaling relationship for the attenuation constant α_{11} (in reciprocal meters):

$$2\alpha_{11} \approx (0.55-0.60)(2a)^{-3}, \quad (1.47)$$

where a is the waveguide radius in centimeters.

A direct method for the determination of the attenuation constant involved a comparison of the powers at the exit and entry of a section of a hollow waveguide of known length excited by the EH_{11} mode generated in a waveguide filter because of the self-filtering effect in hollow-core dielectric waveguides [61]. Our experiments were carried out at a wavelength of 118.8 μm using glass tube waveguides with an internal diameter $2a = 5.5$ and 6.2 mm. In each case we used a filter of the same diameter and the single-mode EH_{11} propagation was established over a distance of ~ 1 m. The measured attenuations were 0.691 and 0.437 m^{-1} , respectively. Hence, we obtained the following relation:

$$2\alpha_{11} \approx (0.055-0.074)(2a)^{-3}, \quad (1.48)$$

which was derived from the experimentally determined values of the attenuation constant by subtracting the measured attenuation of the 118.8 μm radiation in the atmosphere, which amounted to 0.66 dB/m. Comparing (1.47), (1.48) with (1.46), we finally obtain the following scaling relationship:

$$2\alpha_{11} \approx (0.6-0.8)\lambda^2 a^{-3}, \quad (1.49)$$

where λ is the wavelength in millimeters, a is in centimeters, and α_{11} is in reciprocal meters.

Taking into account the weak influence of the dispersion of the refractive index of the waveguide material on α [61], expression (1.49) can be considered valid in the entire THz range for calculating the attenuation constant of the EH_{11} mode, which depends on the geometric dimensions of the waveguide. The total attenuation should include the losses in the medium and should be found – for example – using a table given in [64].

The results of the calculation and experiment, from which the expressions (1.47–1.49) were obtained, are given in the Table 1.1.

Table 1.1

Attenuation of radiation of EH_{11} mode ($\lambda = 337 \mu\text{m}$ and $118.8 \mu\text{m}$) in glass tubes of different diameters

| $\lambda, \mu\text{m}$ | Material | Calculated index of refraction from [65] | Diameter, mm | Attenuation, dB/m | |
|------------------------|----------|--|--------------|-------------------|-------------|
| | | | | Experiment | Calculation |
| 337 | Glass | $n = 2.55 + i 0.18$ | 80 | 0.005 | 0.004 |
| —“— | —“— | —“— | 56 | 0.015 | 0.011 |
| —“— | —“— | —“— | 36 | 0.052 | 0.040 |
| 118.8 | Glass | $n = 2.32 + i 0.40$ | 5.5 | 3 | 1.3 |
| —“— | —“— | —“— | 6.2 | 1.9 | 0.9 |

1.1.4. Transmission of Radiation Wave Beams in Circular Waveguides

Figure 1.8 shows the scheme of the experimental setup. The formation of Gaussian beams with a plane phase front performed by an optical system consisting of a spherical mirror (3) with a radius of curvature of 0.5 m and mirrors (5) with different radii of curvature R . The divergent beam emerging from the THz laser through the coupling hole of diameter 4 mm in the output mirror is incident on spherical mirror (3). The distance l_1 is chosen taking into account the beam divergence in such a way that a beam with a nearly plane phase front is formed in the plane of mirror (5). For the $118.8 \mu\text{m}$ radiation, the distance l_1 is 570 mm, while the distance l_2 between the spherical mirrors 3 and 5 is $l_2 = 1700 \text{ mm}$. The beam diameters d at the level 1/10 of the maximum intensity at the waveguide entrance obtained for different radii of curvature R of mirror (5) are presented in Table 1.2.

Beam diameters were measured by scanning with a pyroelectric detector in a plane perpendicular to the direction of radiation propagation, parallel and perpendicular to the direction of THz radiation polarization. The resolution of the detector used in experiments was 0.2 mm. In order to produce beams of diameter smaller than 2 mm, spherical mirror (5) was replaced by a plane mirror and Teflon lenses 6 of focal length 24, 14 and 9 cm were mounted at a distance of 24 cm from it. In this case, beams of diameter 1.7, 1.3 and 0.9 mm at the 1/10 level of maximum intensity were formed in the waist.

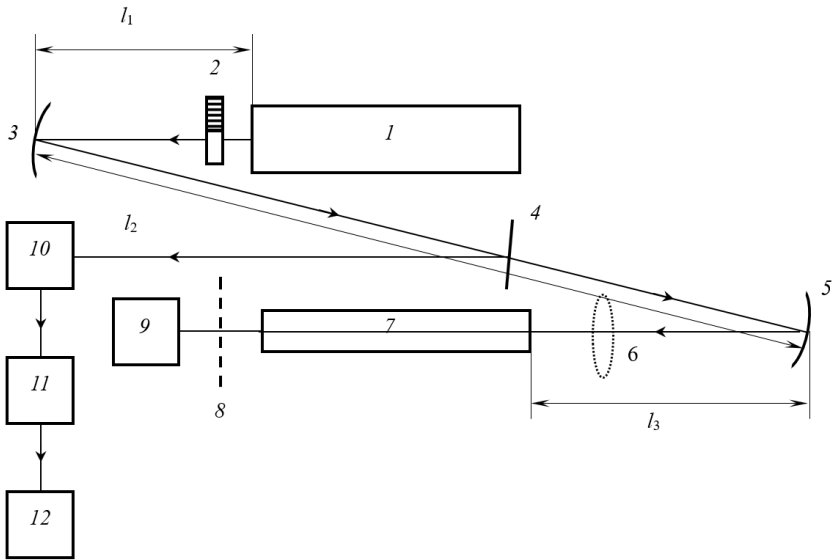


Figure 1.8. Structural diagram of the experimental equipment:
 (1) THz laser; (2) modulator; (3, 5) spherical mirrors;
 (4) divider of THz radiation; (6) lens; (7) waveguide under study;
 (8) polarizer; (9) power meter; (10) pyroelectric receiver;
 (11) measuring amplifier; (12) oscilloscope

Table 1.2

**Dependence of the beam diameter d
 on the radius of curvature R of a mirror**

| R, m | l_3, mm | d, mm |
|--------|-----------|---------|
| 3 | 1160 | 6.5 |
| 2 | 875 | 5.1 |
| 1 | 475 | 3.5 |
| 0.5 | 240 | 2.2 |

The total attenuation δ_{Σ} (in $dB \cdot m^{-1}$) in the waveguide under study was calculated from the expression $\delta_{\Sigma} = \frac{1}{L} 10 \cdot \lg \frac{P_0}{P_1}$, where P_0 and P_1 are the radiation powers at the input and output of the waveguide, respectively; L is the waveguide length. The radiation powers P_0 and P_1 were measured

with a BIM0-1 bolometer with a relative error of $\pm 10\%$. The attenuation of the $118.8\ \mu\text{m}$ radiation was measured taking into account the atmospheric attenuation δ_{atm} , which was determined by measuring the power in two cross sections separated by a distance of $\sim 1\ \text{m}$. The atmospheric attenuation depends on the humidity of air and is not a constant quantity. On different days, it varies in the range $0.5 - 0.7\ \text{dB}\cdot\text{m}^{-1}$. In this case, the attenuation in the waveguide is $\delta_w = \delta_\Sigma - \delta_{\text{atm}}$. The transmission coefficient T was calculated from the attenuation measurements.

The degree of polarisation of radiation was measured by mounting a one-dimensional wire grating polariser at the output of the waveguide. The degree of polarisation Π of the beam was calculated from the expression $\Pi = (P_{\parallel} - P_{\perp}) / (P_{\parallel} + P_{\perp})$, where P_{\parallel} and P_{\perp} are the radiation powers for parallel and perpendicular arrangement of the grating relative to the direction of polarisation of the incident radiation.

The techniques described above were used for computer calculations and experimental measurements of the transmission coefficient and degree of polarisation of radiation in metal (copper) and dielectric (glass) waveguides excited by linearly polarised Gaussian beams from a $118.8\ \mu\text{m}$ CH_3OH laser with a field of type (1.13). Investigations were performed by varying the relative radius w_0 of the initial beam in the range $0.1 - 0.9$ (in its "weak" diffraction region) [55]. The surface resistance of copper taking into account the dc conductivity of the metal $\sigma_0 = 5.73 \times 10^7\ \text{S/m}$ is $R_s = 2.625 \times 10^{-7} \sqrt{c/\lambda}$ [58]. According to [59], at $\lambda = 118.8\ \mu\text{m}$, the theoretical value of the refractive index is $v \approx 216 + i \cdot 576$. Pyrex glass with a theoretical refractive index $v \approx 2.32 + i \cdot 0.40$ at $\lambda = 118.8\ \mu\text{m}$ was chosen as the material for this waveguide [65].

Figure 1.9 shows the results of measurements and calculations of transmission parameters of copper and glass waveguides of identical geometrical dimensions: diameter $2a = 5.7\ \text{mm}$ ($a/\lambda \approx 24$) and length $L = 60\ \text{mm}$. Such a choice of the waveguide length was dictated by the restriction imposed on this parameter in the ray-optics approach and by the need to perform calculations for $L < a^2/\lambda$ [56]. The results presented in the figure demonstrate qualitative agreement between the experimental and theoretical data obtained by using various techniques. This justifies the use of mode approach in the ideal metal approximation at wavelengths exceeding $0.1\ \text{mm}$, and this technique was employed in subsequent calculations.

We studied experimentally and theoretically copper waveguides of different sizes with parameters $2a = 5.7$ mm ($a/\lambda \approx 24$), $L = 500$ mm and $2a = 7.8$ mm ($a/\lambda \approx 33$) and length $L = 400$ mm, as well as glass waveguides with parameters $2a = 5.7$ mm ($a/\lambda \approx 24$), $L = 500$ mm and $2a = 8.5$ mm ($a/\lambda \approx 36$), $L = 500$ mm. Figure 1.10 shows the results of investigation of the transmission coefficient and the degree of polarisation of the output radiation from these waveguides. One can see that unlike dielectric waveguides, the metal waveguides have a transmission coefficient that varies weakly with changing the exciting beam radius and does not have an optimal value. An analysis of the results of calculations by the mode technique shows that for small values of w_0 , the main part of the exciting beam energy is transferred by the higher-order modes that have a weaker attenuation (Figure 1.11). As the value of w_0 increases, the key role in the emission spectrum is played by the TE_{11} and TM_{11} modes with a stronger attenuation than other modes, which explains a decrease in the transmission coefficient for metal waveguides in the case of broad exciting beams. For these cases of excitation Figure 1.12 shows the calculated relative shares of energies in the radiation spectrum of the main waveguide TE and TM modes that arise at the input of a copper waveguide.

The energy fractions of the excited waveguide modes were defined as

$$U_{mn}^{TE} = \frac{(C_{mn})^2}{\sum_{m,n} (C_{mn})^2 + (D_{mn})^2}, \quad U_{mn}^{TM} = \frac{(D_{mn})^2}{\sum_{m,n} (C_{mn})^2 + (D_{mn})^2}.$$

Dielectric waveguides are characterized by a pronounced optimal value of the maximum coefficient of radiation transmission in a waveguide corresponding to the range $0.5 < w_0 < 0.7$, which well agrees with the analogous results obtained during the transmission of single-mode and multimode radiation [55; 56; 66–71].

This optimum corresponds to the transfer of the highest fraction of the exciting beam energy to the fundamental EH_{11} mode of the dielectric waveguide, which has the lowest attenuation (Figure 1.13). Calculated relative fractions of energies in the radiation spectrum of the main waveguide EH_{1m} modes arising at the entrance of a glass waveguide are shown in Fig. 1.14. The energy fractions of the excited waveguide modes were defined as $U_n = (C_n)^2 / \sum_m (C_m)^2$.

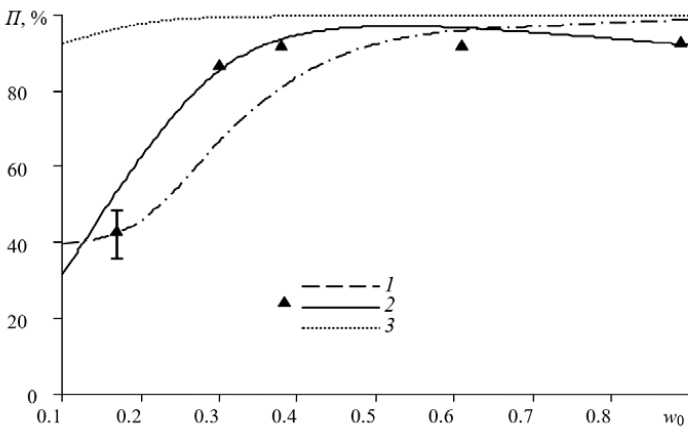
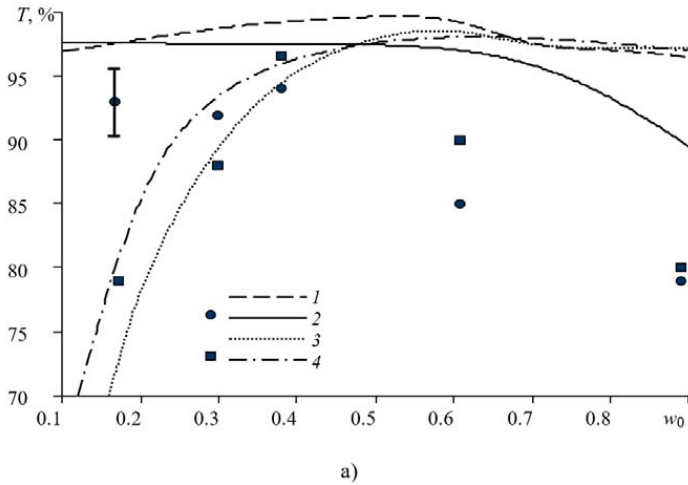


Figure 1.9. Calculated (curves) and experimental (points) dependences of the transmission coefficient T (a) and the degree of polarization Π (b) radiation on the relative radius w_0 of the exciting beam in metallic (1, 2) and dielectric (3, 4) waveguides at $2a = 5.7$ mm, $L = 60$ mm.
 Curves 1, 3 – calculation according to the geometroptic method;
 2, 4 – calculation according to the mode method

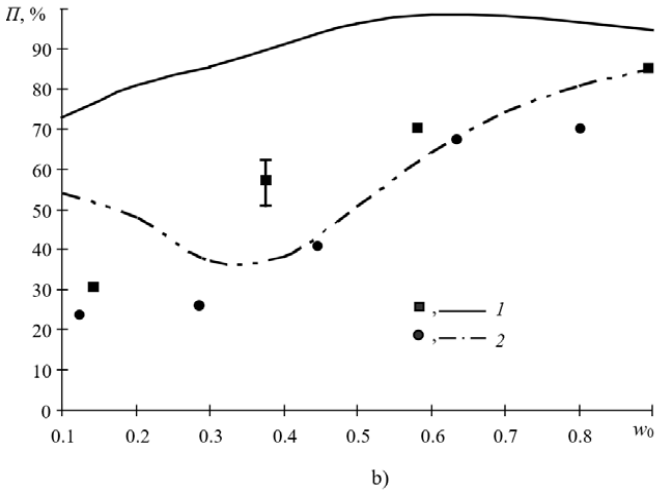
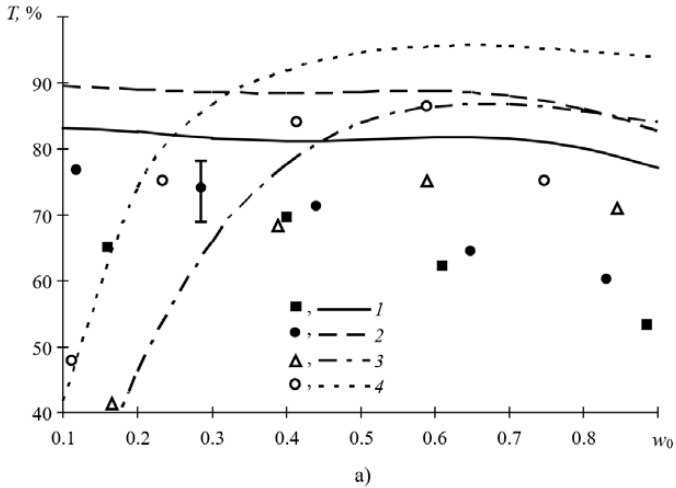


Figure 1.10. Calculated (curves) and experimental (dots) dependences of the transmission coefficient T (a) and the degree of polarization Π (b) of radiation on the relative radius w_0 of the exciting beam in the metal (1, 2) and dielectric (3, 4) waveguides at $2a = 5.7$ mm, $L = 500$ mm (1), $2a = 7.8$ mm, $L = 400$ mm (2), $2a = 5.7$ mm, $L = 500$ mm (3) and $2a = 8.5$ mm, $L = 500$ mm (4)

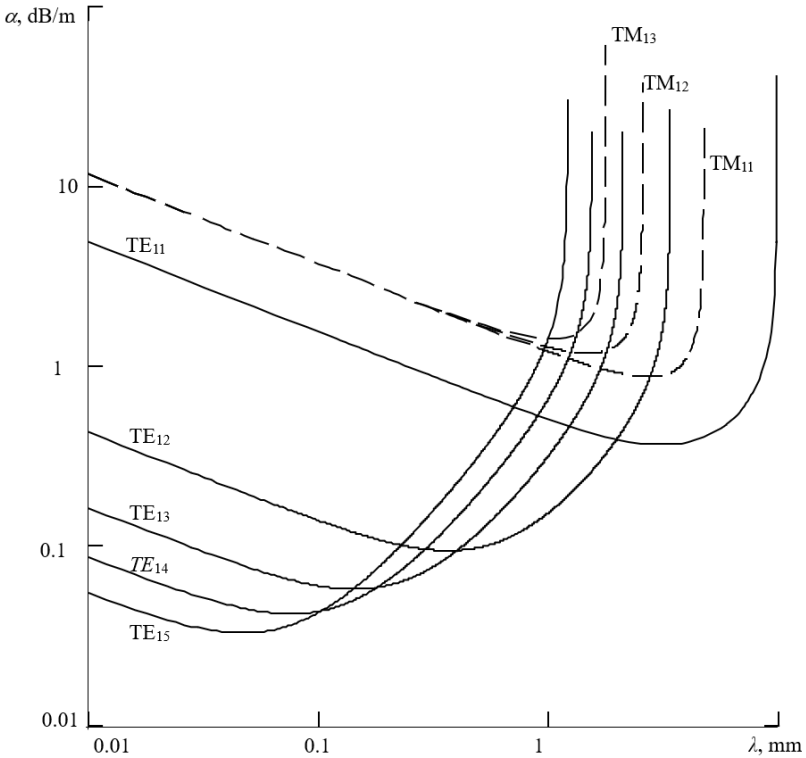


Figure 1.11. Dependence of the attenuation coefficients α TE and TM modes on the wavelength λ of radiation propagating along a circular metal waveguide at $2a = 5.7$ mm

At $w_0 > 0.7$, a significant part of the incident radiation energy does not enter the waveguide, which causes a sharp decrease in the power transmission coefficient for both metal and dielectric waveguides.

For dielectric waveguides, the degree of polarization of the transmitted radiation is close to 100 % and it is well preserved over the entire range of beams under study. In metal waveguides, the degree of polarization of the output radiation increases with an increase in the radius of the exciting beam w_0 and a decrease in and a decrease in a/λ , which is explained by an increase in the contribution of the fundamental waveguide TE_{11} mode

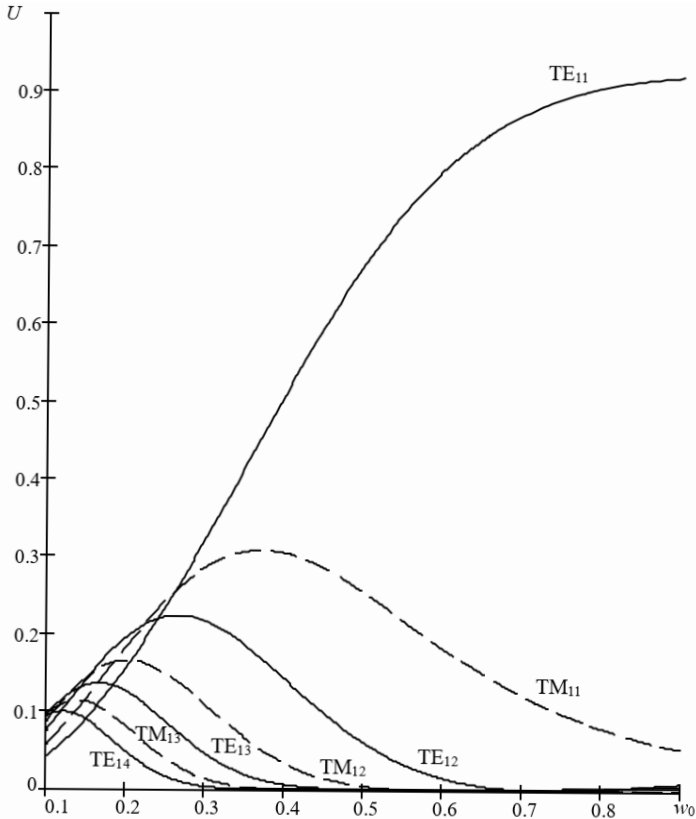


Figure 1.12. Dependencies of the relative fractions of energy U in the radiation spectrum of the main waveguide TE and TM modes excited at the entrance of a circular copper waveguide diameter $2a = 5.7$ mm, from the relative radius of the input beam w_0

(with the maximum fraction of linearly polarized radiation compared to other modes) into the spectral composition of the radiation (Figure 1.14).

Differences in the values of the calculated and experimental data are associated with the irregularity of the cross section, surface roughness and the possible difference between the calculated values of the material constants for the used waveguide.

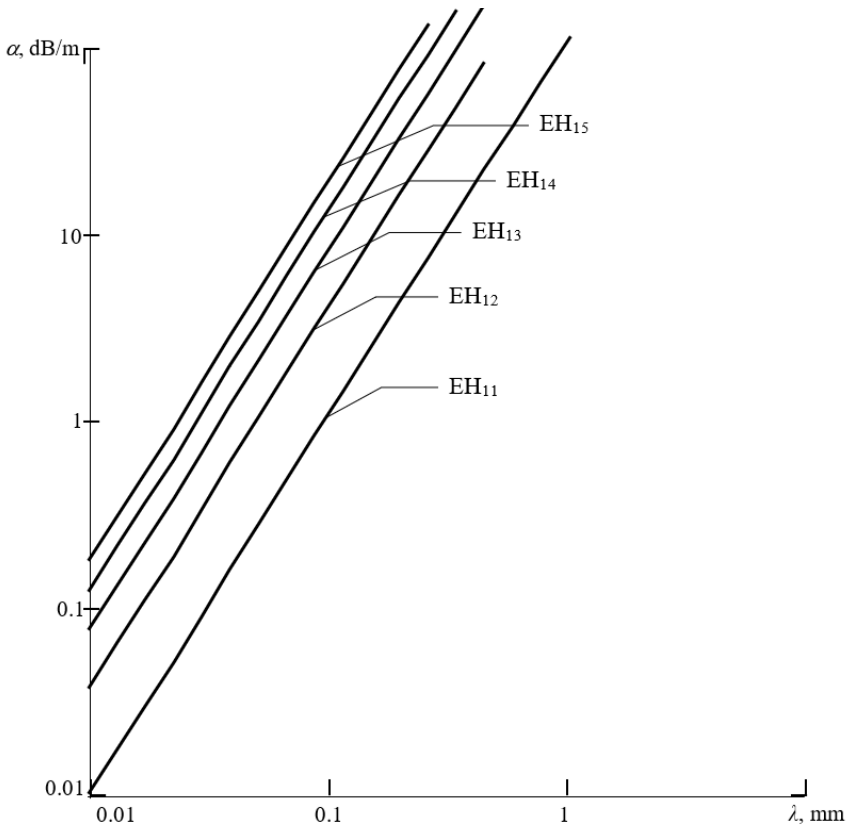


Figure 1.13. Dependence of the attenuation coefficients α of the main waveguide EH_{1m} mode on the wavelength λ in a circular dielectric waveguide with a diameter of $2a = 5.7 \text{ mm}$

An experiment was also carried out on the propagation of Gaussian-like radiation beams in WCD, which are formed in lasers on CH_3OH ($\lambda = 118.8 \mu\text{m}$) and HCN ($\lambda = 337 \mu\text{m}$) molecules with energy output through a central hole in the output reflector. The scheme of the experimental setup and the method of measurements are described in the previous section 1.2.3. The diameter of the exciting beam, the level of curvature of its wavefront, and, accordingly, the coefficients C_m in

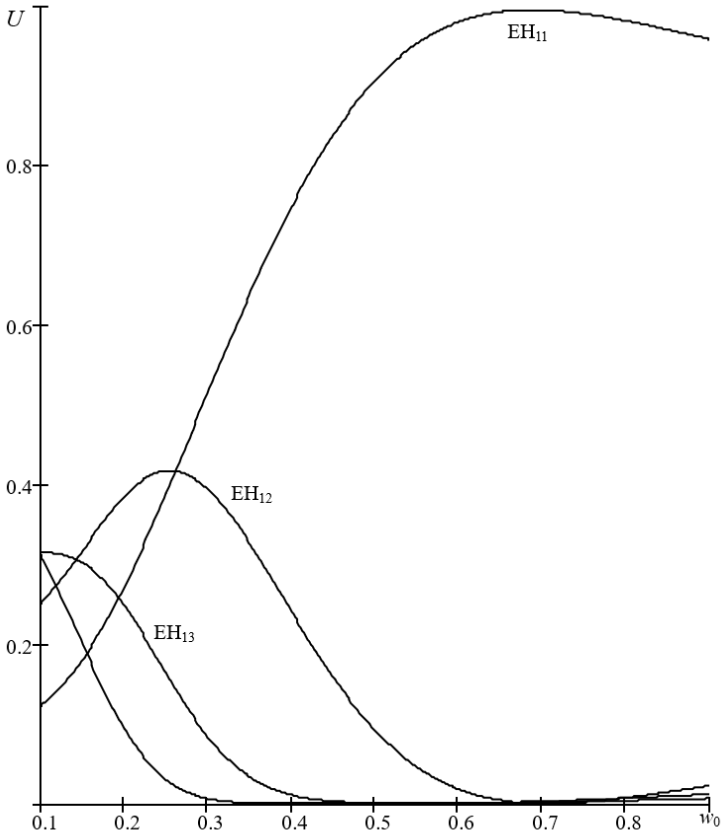


Figure 1.14. Dependencies of the relative fractions of the energy U of the main waveguide EH_{1m} modes in the radiation spectrum excited at the entrance of a circular dielectric waveguide with a diameter of $2a = 5.7$ mm on the relative radius w_0 of the input beam

expression (1.4), which characterize the transfer of beam energy into waveguide modes, change with a change in the distance between the laser output window and the input end of the waveguide. From physical considerations, here, too, one can expect an optimal distance at which the transmission coefficient will have a maximum value. Indeed, both for a

small (relative to the waveguide cross section) beam radius and for a large one, the contribution of higher modes to decomposition (1.4) will be more significant than in some intermediate case.

Figure 1.15 shows the results of measurements at wavelengths of $337 \mu\text{m}$ and $118.8 \mu\text{m}$ and the results of calculations of the transmission coefficient versus the diameter of the exciting beam for glass and quartz tubes of various diameters. In the calculations, the complex amplitudes of the beams exciting the waveguides were found by applying the scalar diffraction operator in the approximation of the Fresnel zone to the complex amplitudes of the fields emitted by the lasers. The latter were obtained by solving the problem of the fundamental mode of resonators for the lasers under study (the solution technique is described in [72]). Moreover, in all the cases under consideration, the radiation beams at the input ends of

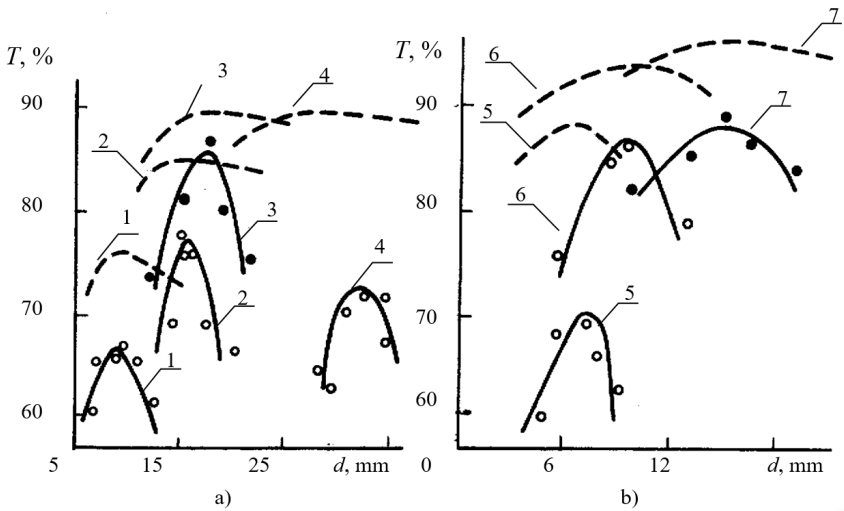


Figure 1.15. Dependence of the radiation transmission coefficient T at the wavelengths $\lambda = 337 \mu\text{m}$ (a) and $118.8 \mu\text{m}$ (b) on the diameter d of the exciting beam in the dielectric waveguides for $2a = 19 \text{ mm}$, $L = 1.09 \text{ m}$ (1), $2a = 30 \text{ mm}$, $L = 1.06 \text{ m}$ (2), $2a = 36 \text{ mm}$, $L = 0.86 \text{ m}$ (3), $2a = 56 \text{ mm}$, $L = 1.32 \text{ m}$ (4), $2a = 13 \text{ mm}$, $L = 1.34 \text{ m}$ (5), $2a = 19 \text{ mm}$, $L = 1.05 \text{ m}$ (6), $2a = 30 \text{ mm}$, $L = 1.01 \text{ m}$ (7).

Solid curves – experiment, dotted curves – calculation

the waveguides had the shape of the field intensity distribution close to the Gaussian curve. It follows from the calculated data that the optimal ratio of the exciting beam radius to the waveguide radius is in the range $p = 0.4\text{--}0.5$. These results are close to the theoretical values of the optimal excitation of the EH_{11} mode $d/D = 0.455$ [66–68] and to the experimental values for a Gaussian beam with a waist at the waveguide input $0.20 < d/D < 0.55$ [57; 70].

1.1.5. Reconstruction of Gaussian Radiation Beams in Metal Circular Waveguides

Let a monochromatic light source with electric field distribution $E_0(\rho)$ be excite the input face of a circular waveguide ($z = 0$). This distribution can be represented as a superposition of an infinite set of the waveguide wave functions $F_m(\rho)$ with the amplitudes a_m :

$$E_0(\rho) = \sum_{m=1}^{\infty} a_m F_m(\rho) . \quad (1.50)$$

The field distribution in an arbitrary waveguide section $z \gg \lambda$ is also determined by the superposition of the waveguide wave functions. However, in contrast to the cross

section $z = 0$, this superposition takes into account the difference in propagation constants of different modes γ_m and the number of terms in the series is limited:

$$E_z(\rho) = \exp(i\gamma_1 z) \sum_{m=1}^M a_m F_m(\rho) \exp[iz(\gamma_m - \gamma_1)], \quad (1.51)$$

where M is the number of the limiting mode of the waveguide.

If now such a section $z = L$ exists, where the phase ratio between any modes is a multiple of 2π :

$$\exp[iL(\gamma_m - \gamma_1)] = 1, \quad (1.52)$$

then this section can be called equiphase section. In this section, mode superposition (1.51) reproduces the input distribution $E_0(\rho)$ with an accuracy determined by the number of allowed waveguide modes. It is clear that if there is one equiphase cross section, then in the case of ideal waveguides there should be an infinite number of them. Any section that satisfies the condition $z_g = gL$ ($g = 0, 1, 2, \dots$) will also be equiphase. Thus, the possibility of image transmission through a multimode waveguide is determined by the

specific type of characteristic spectrum of propagation constants γ_m for this waveguide.

As is known, the propagation of two sets of TM and TE-waves (corresponding to two main directions of polarization) is possible in metal waveguides. Waves excited in a given waveguide by a certain radiation source are, in essence, components of the expansion of the field of this source in terms of waveguide eigenwaves. Since waves of different modes propagate in the waveguide with different phase velocities $v_m = c[1 - (\lambda / \lambda_m)^2]^{-1/2}$ (where c is the speed of light in the waveguide, λ_m is the critical wavelength of the mode with the index m), then in an arbitrary section of the waveguide $z > 0$ their superposition does not repeat the distribution fields of the radiation source in the cross section $z = 0$.

The initial field distribution of the radiation source cannot be reproduced exactly in the equiphase section for the following main reasons:

- in the general case of an arbitrarily complex structure of the initial field, the latter cannot be represented as the sum of a finite number of terms, limited by the waveguide limiting condition $\lambda / \lambda_m < 1$;
- the attenuation in the waveguide depends on the mode index, as a result of which the ratio of the expansion amplitudes in terms of the waveguide eigenfunctions in the equiphase plane z_g does not coincide with the initial ones at $z = 0$.

However, in the paraxial case, when $(\lambda / \lambda_m)^2 \ll 1$, there are such sections $z_g > 0$, where the phase relation between individual modes coincides with the initial one at $z = 0$ with a sufficient degree of accuracy or differs from it by an amount that is a multiple of 2π . Consequently, in these sections $z = z_g$, defined as equiphase, the summation of the expansion components occurs so that the mode superposition creates an image of the initial field of the radiation source that excites the waveguide in the section $z = 0$. Such waveguide, in accordance with its ability to decompose monochromatic fields in terms of eigenfunctions, transfer the expansion terms to a remote point, and there synthesize the initial field distribution from them, is called a polyharmonic waveguide [73].

With regard to the terahertz range, the problem of studying the features of image transmission by metal waveguides with cross-sectional dimensions significantly exceeding the oscillation wavelength and a relatively large number of allowed modes is an actual problem.

Based on the mode paraxiality condition, let us estimate the location of equiphase cross sections in a circular metal waveguide. A circular waveguide with a diameter of $2a$ has a set of TE and TM modes [51] described by Bessel functions, and their critical wavelengths are equal to $\lambda_k^{TE} = \frac{2\pi a}{\chi_{mn}}$; χ_{mn} is the n -th root of the equation $J'_m(\chi) = 0$, $\lambda_k^{TM} = \frac{2\pi a}{\eta_{mn}}$, η_{mn} is the n -th root of the equation $J_m(\eta) = 0$. The phase difference between the waves of any two modes with indices p, l and q, k acquired on the length of the waveguide, is equal to

$$\Phi_{pl,qk}(z) \approx 2\pi \frac{z}{\lambda} \left[\sqrt{1 - \left(\frac{\lambda}{\lambda_{pl}} \right)^2} - \sqrt{1 - \left(\frac{\lambda}{\lambda_{qk}} \right)^2} \right]. \quad (1.53)$$

The phase difference for the paraxial case, when $(\lambda/\lambda_{pl,qk})^2 \ll 1$ and we can restrict ourselves to the second terms of the expansion of the roots, for example, in the case of TE modes, is equal to

$$\Phi_{pl,qk}(z) = 2\pi \frac{z}{\lambda} \left[\frac{1}{2} \left(\frac{\lambda}{\lambda_{qk}} \right)^2 - \frac{1}{2} \left(\frac{\lambda}{\lambda_{pl}} \right)^2 \right] = 2\pi \frac{z\lambda}{8\pi a^2} [\chi_{qk}^2 - \chi_{pl}^2]. \quad (1.54)$$

In the general case, the difference of the squares of the roots does not form an integer (or a constant fraction of an integer), which excludes the possibility of an equiphase cross section. If, however, we confine ourselves to the case when it is possible to represent the roots in the form of series [74]

$$\chi_{pl} \approx \pi \left[l + \frac{p}{2} + \frac{1}{4} \right] \left[1 - \frac{4p^2 + 3}{8\pi^2(l + (p/2) + (1/4))^2} - \dots \right], \quad (1.55)$$

$$\eta_{pl} \approx \pi \left[l + \frac{p}{2} - \frac{1}{4} \right] \left[1 - \frac{4p^2 - 1}{8\pi^2(l + (p/2) - (1/4))^2} - \dots \right] \quad (1.56)$$

and keep only the first terms in them, then for the phase difference we obtain

$$\Phi_{pl,qk}(z) \approx 2\pi \frac{z\lambda}{32a^2} \left[2(2k + 2l \pm 1)(k - l) + (q + p \pm 1)(q - p) + 4(kq - lp) \right], \quad (1.57)$$

where the + sign applies only to TE, and the minus sign applies to TM modes, and

$$\begin{aligned} \Phi_{pl,qk}(z) \approx 2\pi \frac{z\lambda}{32a^2} [2(2k - 2l - 1)(k + l) + \\ + (q - p - 1)(q + p) + 4(kq - lp)], \end{aligned} \quad (1.58)$$

when the phase difference between the TE and TM modes is calculated.

It is easy to see that the quantity in square brackets in (1.57) and (1.58) is always even for any values of indices p, l, q, k . Thus, the main equiphase cross sections for a circular metal waveguide lie at distances

$$z = z_g = \frac{16a^2}{\lambda} g, \quad (g = 0, \pm 1, \pm 2\dots). \quad (1.59)$$

Having calculated the radiation intensity at the observation point as $I(\rho, \phi, z) = |E(\rho, \phi, z)|^2$, we will estimate the error in restoring the original beam using the normalized absolute average measure of the difference between images introduced in [60]:

$$\delta = \frac{\sum_{i,j} \left| |E'(\rho_i, \phi_j, z)|^2 - |E_0'(\rho_i, \phi_j)|^2 \right|}{\sum_{i,j} |E_0'(\rho_i, \phi_j)|^2}, \quad (1.60)$$

where E' and E_0' are distributions of the field amplitude of the output and input beams normalized to the maximum. Indices i, j display the number of points for numerically specifying functions.

The considered beam of the form (1.2) effectively excites only a few lower modes in a circular metal waveguide. It is confirmed by the results of calculations given in Table 1.3, where $u_n^{TE} = |C_n|^2 / \sum_{m=1}^M |C_m|^2 \cdot 100\%$, $u_n^{TM} = |D_n|^2 / \sum_{m=1}^M |D_m|^2 \cdot 100\%$ are the coefficients characterizing the relative fractions of the energy of the waveguide TE and TM modes excited in the waveguide by a Gaussian beam of radiation with a radius w_0 .

When a Gaussian beam is transmitted through a waveguide, energy is transferred from higher waveguide modes to lower ones. It is confirmed by the data in the Table 1.3 where

$$v_{1n}^{TE} = |C_n|^2 \exp(-2\alpha_{1n}^{TE} \cdot L) / \left| \sum_{m=1}^M |C_m|^2 \exp(-2\alpha_{1m}^{TE} \cdot L) \right| \cdot 100 \%,$$

$$v_{1n}^{TM} = |D_n|^2 \exp(-2\alpha_{1n}^{TM} \cdot L) / \left| \sum_{m=1}^M |D_m|^2 \exp(-2\alpha_{1m}^{TM} \cdot L) \right| \cdot 100 \%,$$

are the coefficients characterizing the relative fraction of the energy of the waveguide TE and TM modes at the output of the waveguide when it is excited by a radiation beam of radius w_0 . The calculation was carried out for a waveguide with a diameter of $2a = 5.7$ mm and a length of 500 mm ($\lambda = 0.1188$ mm). It follows from the data in the Table that, due to different attenuation of the waveguide modes, the ratio of the amplitudes of the TM and TE modes in the output beam changes in favor of the latter, i.e. the waveguide acts as a polarizer.

Figure 1.16 shows the field intensity distributions in the waveguide sections, characterized by the dimensionless length parameter $g = z/\lambda^2$. The curves were obtained by calculations on a computer with $w_0 = 0.6$ ($a/\lambda = 24$). Sections are visible in which the intensity of the input distribution is repeated ($g = 0$).

According to (1.59), in the case of paraxial approximation, when images are transmitted in a circular waveguide, the first self-image plane of the input distribution corresponds to the parameter value $g = 16$. In real waveguides, due to the attenuation of the TM and TE modes, the imaging occurs at a closer distance from the end of the waveguide, corresponding to $g \approx 7$. As can be seen from Figure 1.16, if parameter g deviates from the value at which the specified imaging is observed, the field distribution can be significantly distorted.

Results were obtained that are similar to those shown in Fig. 1.16, for a set of values a/λ . For each of these values, the calculations were carried out with a set of w_0 values. For fixed a/λ and w_0 , the values of the relative length parameter g were found, at which the input field is repeated. The results are shown in Table 1.4 for a radiation beam with $\lambda = 0.1188$ mm. The given values correspond to the errors of representing the input field as a sum of waveguide modes and imaging the distribution of this field in the cross-section $z = g(a^2/\lambda)$, which does not exceed 10 %.

Table 1.3

Relative fractions of the energy of waveguide TE and TM modes in the beam at the entrance and exit of a circular metal waveguide excited by a Gaussian radiation beam of radius w_0

| w_0 | | 0.2 | | 0.4 | | 0.6 | | 0.8 | |
|---------------|---------------|------|------|------|------|------|------|------|------|
| u_{11}^{TE} | v_{11}^{TE} | 15.7 | 41.6 | 50.9 | 71.7 | 76.2 | 83.3 | 82.9 | 83.9 |
| u_{12}^{TE} | v_{21}^{TE} | 19.6 | 14.8 | 14.3 | 9.0 | 2.8 | 1.7 | 0.8 | 0.4 |
| u_{13}^{TE} | v_{13}^{TE} | 12.6 | 6.8 | 0.7 | 0.6 | 0 | 0.1 | 0.1 | 0.1 |
| u_{11}^{TM} | v_{11}^{TM} | 18.4 | 14.4 | 30.6 | 12.5 | 20.8 | 12.7 | 16.1 | 13.8 |
| u_{12}^{TM} | v_{12}^{TM} | 16.6 | 12.2 | 3.5 | 6.0 | 0.1 | 2.0 | 0 | 1.4 |
| u_{13}^{TM} | v_{13}^{TM} | 8.1 | 4.2 | 0.1 | 0.1 | 0 | 0.2 | 0 | 0.2 |

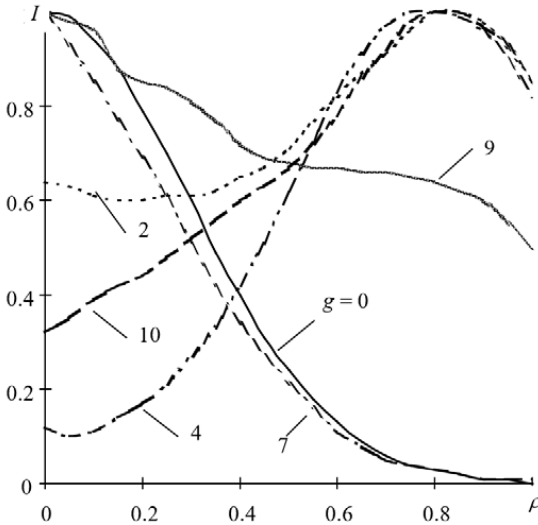


Figure 1.16. Calculated relative transverse field intensity distributions at the entrance ($g = 0$) and exit of a metal waveguide with a diameter of $2a = 5.7$ mm and a length of $L = ga^2/\lambda$. when it is excited by a Gaussian beam with relative radius $w_0 = 0.6$

CHAPTER 1

The meaning of the intervals in the Table 1.4 for the parameters w_0 and g is that the imaging of the input field with the specified error is possible only for the values w_0 and g from these intervals. For example, at $a/\lambda = 25$, for each of the radiation beams with the parameter w_0 from the range of 0.46...0.75, at least one section in the waveguide can be found from the set $z = ga^2/\lambda$, $g = 6.01...7.08$, where the field distribution coincides with the input distribution with an error of no more than 10 %, i.e. condition (1.60) $\delta \leq 0.10$ is satisfied. Also in Table 1.4, for a given a/λ the value of the beam radius $w_{0 \text{ opt}}$, the location of its reconstruction cross section g_{opt} and the attenuation value Z are presented, for which the above error δ is the minimum. The value of the degree of polarization of the output radiation, calculated by formula (1.7), is also given here. Similar data on the conditions for the self-imaging of a radiation beam that excites a waveguide with a Gaussian field distribution at $\lambda = 0.4326$ mm are given in Table 1.5.

Table 1.4

**Self-imaging conditions of radiation Gaussian beams
of the lowest order in circular metal waveguides ($\lambda = 0.1188$ mm)**

| a/λ | 25 | 50 | 75 | 100 |
|---------------------|-----------|-----------|-----------|------------|
| w_0 | 0.46–0.75 | 0.46–0.79 | 0.48–0.82 | 0.54–0.77 |
| g | 6.01–7.19 | 6.02–7.20 | 6.31–7.22 | 6.48–7.08 |
| L , m | 0.45–0.53 | 1.79–2.14 | 4.22–4.82 | 7.70–8.41 |
| $w_{0 \text{ opt}}$ | 0.60 | 0.62 | 0.65 | 0.65 |
| g_{opt} | 6.69 | 6.88 | 6.84 | 6.88 |
| δ , % | 2.85 | 4.41 | 5.95 | 7.06 |
| Z , dB | 1.4 | 2.33 | 3.26 | 4.04 |
| Π , % | 97.15 | 97.79 | 97.59 | 97.02 |

The content of the intervals in the tables for parameters w_0 and g is that the display of the input field with the specified error is possible only for the values of w_0 and g from the specified intervals. For example, at $a/\lambda = 25$, for each of the radiation beams with the parameter w_0 from the range of 0.46...0.75, at least one section in the waveguide can be found from the set $z = ga^2/\lambda$, $g = 6.01...7.08$, where the field distribution coincides with the input distribution with an error of no more than 10 %, i.e. condition (1.60) $\delta \leq 0.10$ is satisfied. Also in Table 1.4, for a given a/λ the value of the beam radius $w_{0 \text{ opt}}$, the location of its reconstruction cross

section g_{opt} and the attenuation value Z are presented, for which the above error δ is the minimum. The value of the degree of polarization of the output radiation, calculated by formula (1.7), is also given here. Similar data on the conditions for the self-imaging of a radiation beam that excites a waveguide with a Gaussian field distribution at $\lambda = 0.4326$ mm are given in Table 1.5.

Table 1.5

**Self-imaging conditions of radiation Gaussian beams
of the lowest order in circular metal waveguides ($\lambda = 0.4326$ mm)**

| a/λ | 25 | 50 | 75 | 100 |
|--------------|-----------|-----------|-----------|------------|
| w_0 | 0.45-0.75 | 0.45-0.76 | 0.46-0.77 | 0.47-0.75 |
| g | 6.01-7.08 | 6.02-7.20 | 6.02-7.22 | 6.27-7.09 |
| L, m | 1.63-1.91 | 6.5-7.8 | 14.6-17.6 | 27.1-30.7 |
| $w_{0, opt}$ | 0.59 | 0.60 | 0.61 | 0.60 |
| g_{opt} | 6.68 | 6.59 | 6.71 | 6.79 |
| $\delta, \%$ | 2.66 | 3.21 | 3.84 | 4.74 |
| Z, dB | 0.94 | 1.41 | 1.90 | 2.28 |
| $\Pi, \%$ | 97.05 | 96.89 | 97.07 | 97.15 |

1.2. TRANSMISSION AND SELF-IMAGING OF GAUSSIAN RADIATION BEAMS IN METALLIC RECTANGULAR WAVEGUIDES

1.2.1. Modal Calculation Technique

Let a linearly polarised axially symmetric Gaussian radiation beam be incident on the input face of a waveguide directed along the z axis and having dimensions $2a \times 2b$ ($a > b$) in the transverse plane x, y so that its polarisation vector is directed along the broad or narrow wall of the waveguide (Figure 1.17). The electric field $\vec{E}_0 = E_0(x, y, 0) \cdot \vec{x}_0$ or $\vec{E}_0 = E_0(x, y, 0) \cdot \vec{y}_0$ in the plane $z = 0$ of the source has the form

$$E_0(x, y, 0) = \left(\frac{2}{\pi}\right)^{1/2} \exp\left(-\frac{x^2 + y^2}{w_0^2}\right), \quad (1.61)$$

where \vec{x}_0, \vec{y}_0 are the unit vectors of Cartesian coordinates in x and y directions, and w_0 is the beam radius at the $1/e$ level of the maximum amplitude.

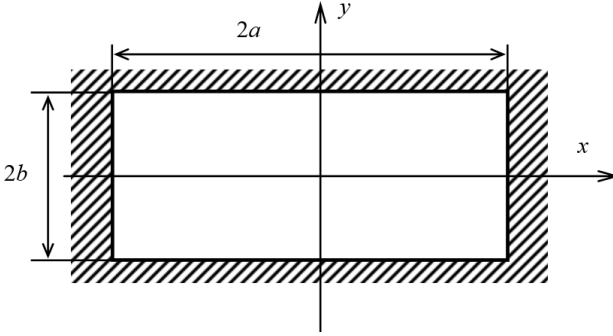


Fig. 1.17 Rectangular waveguide cross section

Similar to the mode consideration in subsection 1.1.1.2, the transverse components of the input field in a metal waveguide can be represented as a series expansion in orthogonal waveguide TE and TM modes. In our case, the normalised transverse components of the electric field for waves in a rectangular waveguide have the form:

$$\begin{aligned} \vec{V}_{mn}^{TE}(x, y) = & \vec{x}_0 \cdot \frac{1}{2b} \frac{n\sqrt{\epsilon_m \epsilon_n}}{\sqrt{m^2 \frac{b}{a} + n^2 \frac{a}{b}}} \cos\left[\frac{m\pi}{a}(x+a)\right] \sin\left[\frac{n\pi}{b}(y+b)\right] - \\ & - \vec{y}_0 \cdot \frac{1}{2a} \frac{m\sqrt{\epsilon_m \epsilon_n}}{\sqrt{m^2 \frac{b}{a} + n^2 \frac{a}{b}}} \sin\left[\frac{m\pi}{a}(x+a)\right] \cos\left[\frac{n\pi}{b}(y+b)\right], \quad (1.62) \end{aligned}$$

where $m, n = 0, 1, \dots$ (the $m = n = 0$ mode does not exist),

$$\epsilon_{m,n} = \begin{cases} 1 & \text{for } m, n = 0, \\ 2 & \text{for } m, n \neq 0; \end{cases}$$

$$\begin{aligned} \vec{V}_{mn}^{TM}(x, y) = & -\vec{x}_0 \cdot \frac{1}{a} \frac{m}{\sqrt{m^2 \frac{b}{a} + n^2 \frac{a}{b}}} \cos\left[\frac{m\pi}{a}(x+a)\right] \sin\left[\frac{n\pi}{b}(y+b)\right] - \\ & - \vec{y}_0 \cdot \frac{1}{b} \frac{n}{\sqrt{m^2 \frac{b}{a} + n^2 \frac{a}{b}}} \sin\left[\frac{m\pi}{a}(x+a)\right] \cos\left[\frac{n\pi}{b}(y+b)\right], \quad (1.63) \end{aligned}$$

where $m, n = 1, 2, 3, \dots$

Scientific monograph

The series expansion of the original field in terms of the system of orthogonal functions introduced above has the form

$$\vec{E}_0(x, y, 0) = \sum_{m,n} C_{mn} \vec{V}_{mn}^{TE}(x, y) + \sum_{m,n} D_{mn} \vec{V}_{mn}^{TM}(x, y), \quad (1.64)$$

where the amplitudes C_{mn} and D_{mn} of the modes excited at the waveguide input are defined by the relations

$$C_{mn} = \int_{-a}^a \int_0^b \vec{E}_0(x, y, 0) \vec{V}_{mn}^{TE}(x, y) dx dy.$$

In this case, the field distribution over the waveguide cross section at a distance L from the input face is

$$\vec{E}(x, y, L) = \sum_{m,n} C_{mn} \vec{V}_{mn}^{TE}(x, y) \exp(i\gamma_{mn}^{TE} L) + \sum_{m,n} D_{mn} \vec{V}_{mn}^{TM}(x, y) \exp(i\gamma_{mn}^{TM} L), \quad (1.65)$$

where $\gamma_{mn}^{TE} = \beta_{mn} + i\alpha_{mn}^{TE}$, $\gamma_{mn}^{TM} = \beta_{mn} + i\alpha_{mn}^{TM}$ are the propagation constants for TE and TM mode [51]:

$$\beta_{mn} = 2\pi \sqrt{\left(\frac{1}{\lambda^2} - \frac{1}{\lambda_k^2}\right)},$$

$$\alpha_{mn}^{TM} = \frac{R_s}{R_0 \cdot a} \frac{1}{\sqrt{1 - \left(\frac{\lambda}{\lambda_k}\right)^2}} \left(\frac{m^2 + n^2 \frac{a^3}{b^3}}{m^2 + n^2 \frac{a^2}{b^2}} \right),$$

$$\alpha_{mn}^{TE} = \frac{R_s}{2R_0 \cdot b} \left[\frac{\mu_n m^2 \frac{b}{a} + \mu_m n^2}{m^2 \frac{b}{a} + n^2 \frac{a}{b}} \sqrt{1 - \left(\frac{\lambda}{\lambda_k}\right)^2} + \frac{\left(\mu_n + \mu_m \frac{b}{a}\right) \left(\frac{\lambda}{\lambda_k}\right)^2}{\sqrt{1 - \left(\frac{\lambda}{\lambda_k}\right)^2}} \right],$$

$$\lambda_k = \frac{2}{\sqrt{\left(\frac{m}{2a}\right)^2 + \left(\frac{n}{2b}\right)^2}} \text{ is the critical wavelength, } \lambda \text{ is the wavelength}$$

in free space, $R_0 = 376.73 \Omega$ is the wave resistance of free space, R_s is the surface resistance of the waveguide material.

The radiation power passing through the cross section is

$$P_{out}(L) = \sum_{mn} |C_{mn}|^2 \exp(-2\alpha_{mn}^{TE}L) + \sum_{mn} |D_{mn}|^2 \exp(-2\alpha_{mn}^{TM}L). \quad (1.66)$$

The above relations allow us to determine the coefficient of radiation transmission in the waveguide and the degree of polarisation of the output radiation by the formula (1.7).

Following the analysis carried out in [73; 75], we consider the fulfillment of conditions (1.52) of restoring the transverse field distribution for an initial radiation beam of the form (1.61) in the rectangular metal waveguide under consideration, whose characteristic spectrum of phase constants for the TE and TM modes has the form:

$$\beta_{mn} = 2\pi \sqrt{\left(\frac{1}{\lambda}\right)^2 - \left(\frac{1}{\lambda_{mn}}\right)^2}.$$

In this case, the phase difference φ between the waves of any two modes with arbitrary indices mn and kl in the paraxial case is

$$\phi_{mn,kl} \approx 2\pi \frac{z\lambda}{32a^2} \left[k^2 - m^2 + \left(\frac{a}{b}\right)^2 (l^2 - n^2) \right]. \quad (1.67)$$

In a rectangular waveguide with an integer ratio of transverse dimensions (a/b), the sum in square brackets is also an integer number. From the condition of the multiple 2π of the phase difference between the modes, we find that the equality

$$z_s = \left(\frac{32a^2}{\lambda}\right)s, \quad s = 1, 2, 3, \dots$$

defines a sequence of in-phase sections z_s for a rectangular metal waveguide, in which the superposition of paraxial modes reproduces the shape of the input field.

Apart from the basic equiphase sections z_s additional cross sections may also exist for special types of excitation. Consider the special types of excitation that are important for our analysis. Suppose that the excitation spectrum of a rectangular waveguide with an integer ratio of transverse dimensions contains only waveguide TE_{mn} and TM_{mn} modes with an even number of half-waves of the field between the center and the wall of the

waveguide in the direction of the x -axis (see Figure 1.17), which are denoted by the index m and an odd number half-waves between the center and the wall of the waveguide in the direction of the y -axis, which are denoted by the index n . Then it is easy to show from (1.67) that in this case the in-phase sections are located at distances $z_s = (8a^2 / \lambda)s$. If, however, the excitation spectrum contains modes with an odd index m and an even index n , the equiphase cross sections are located at distances $z_s = (4a^2 / \lambda)s$.

However, the above expressions can be used only to predict the approximate position of equiphase cross sections. The reasons for this are explained in [73; 75]. The spectral technique described above must be used for a more precise evaluation of the position z_s of cross sections for reconstruction of the Gaussian THz radiation and estimation of the error in such a reconstruction.

1.2.2. Comparison of Experimental and Numerical Results

Experiments were performed using the setup described in section 1.1.4, the only difference being in the radiation source, which in our case was an optically pumped 432.6 μm THz formic acid (HCOOH) laser. For radii of curvature of mirror (5) equal to 100 and 50 cm, the laser beam diameters at the 1/10 level of the maximum intensity were 6.2 and 3.8 mm, respectively. To produce beams of a smaller diameter, spherical mirror (5) was replaced by a plane mirror and Teflon lenses (6) of focal lengths 24, 14 and 19 cm were mounted at a distance of 24 cm from this mirror. This resulted in the formation of beams of diameters 4.4, 3.2 and 2.7 mm, respectively, at the waist. Measurements of beam diameter, transmission coefficient, and degree of polarisation of radiation were made in the same way as in section 1.1.4.

The proposed technique was used for computer calculations and experimental measurement of the transmission coefficient and degree of polarisation of radiation in rectangular copper waveguides excited by linearly polarised Gaussian beams of THz laser radiation with a field of type (1.61). The relation $R_s = 2.625 \cdot 10^{-7} (c/\lambda)^{1/2}$ was used in calculations to take into account the surface resistance of copper [76]. The relative beam radius $w = w_0/a$ was varied in the interval 0.1 – 0.9 (in the region of its "weak" diffraction [55]).

Figure 1.18 shows the results of theoretical and experimental studies of the dependence of radiation transmission coefficient T on the relative radius

w of a beam entering a copper waveguide of dimensions $11 \times 5.5 \text{ mm}^2$ and $L = 500 \text{ mm}$. The polarization vector of the beam is directed along the broad and narrow walls of the waveguide. The energy fractions of the excited waveguide modes were defined as

$$U_{mn}^{TE} = \frac{(C_{mn})^2}{\sum_{m,n} (C_{mn})^2 + (D_{mn})^2}, \quad U_{mn}^{TM} = \frac{(D_{mn})^2}{\sum_{m,n} (C_{mn})^2 + (D_{mn})^2}.$$

Figure 1.19 shows the calculated relative energy fractions in the emission spectrum of the basic TE and TM waveguide modes emerging at the waveguide input for such excitations. It can be seen that for rectangular metal waveguides, with increasing w , a slight increase in the radiation transfer coefficient is first observed, and at values of w greater than 0.5, its decrease is noted. The increase in the transmission coefficient with w is explained by the fact that the relative fraction of energy of the fundamental waveguide modes having a lower attenuation than the other modes increases in the input radiation spectrum.

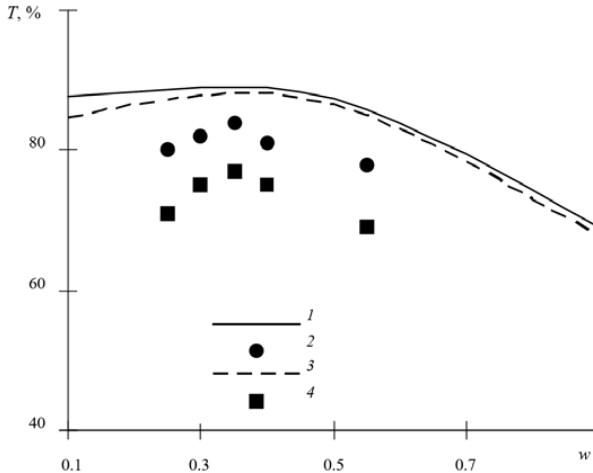


Figure 1.18. Calculated (1, 3) and experimental (2, 4) dependences of the radiation transmission coefficient T on the relative radius w of the excitation beam linearly polarized along the wide (1, 2) and narrow (3, 4) walls in a copper waveguide with dimensions $2a = 11 \text{ mm}$, $2b = 5.5 \text{ mm}$, $L=500 \text{ mm}$

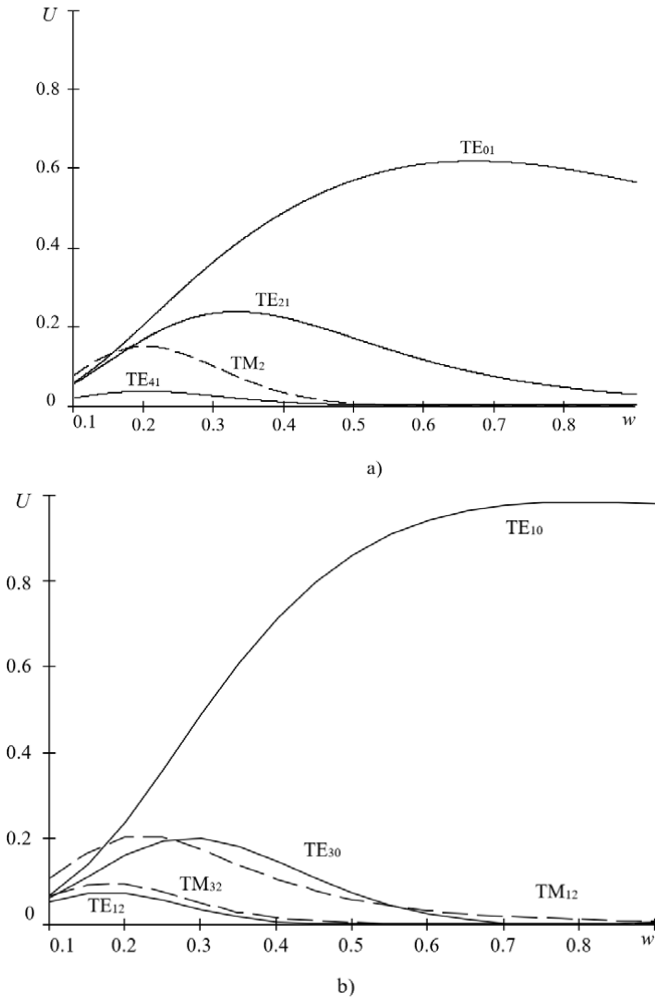


Figure 1.19. Relative fractions of energy U in the radiation spectrum of the fundamental waveguide TE and TM modes excited at the entrance of a rectangular copper waveguide with dimensions $2a = 11$ mm and $2b = 5.5$ mm, from the relative radius w of the exciting beam linearly polarized along the wide (a) and narrow (b) waveguide walls

CHAPTER 1

This is confirmed by calculations presented in Figure 1.20, which contains the transmission coefficient of radiation for the fundamental eigenmodes of the waveguide under study. The decrease in T for $w > 0.5$ is observed because a part of the beam energy does not enter the waveguide.

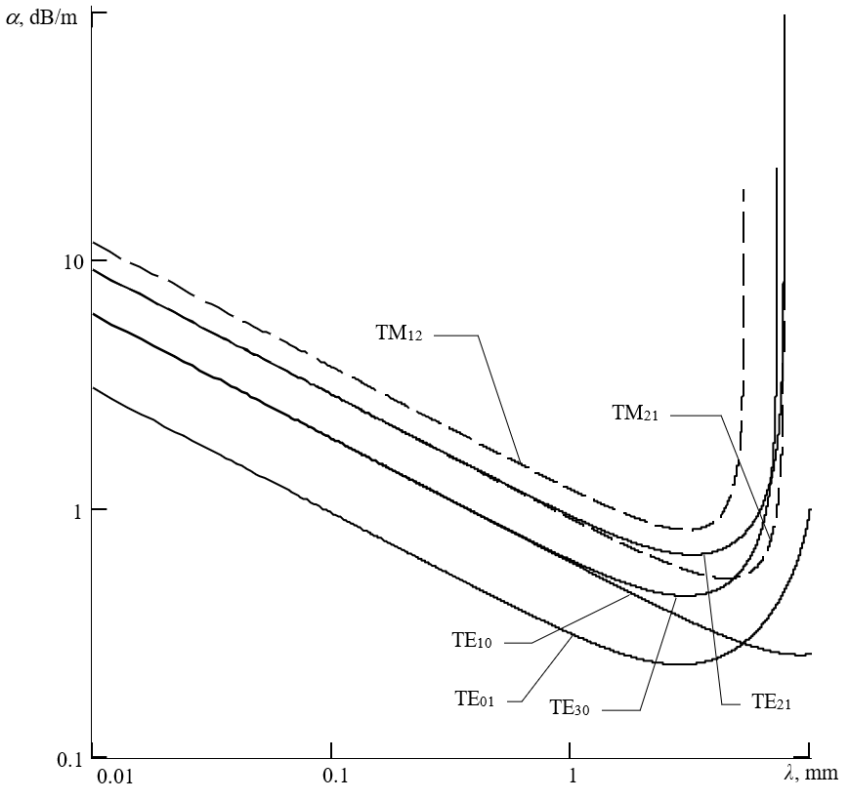


Figure 1.20. Dependence of the attenuation coefficients α of the main waveguide TE and TM modes on the wavelength λ in a rectangular metal waveguide with dimensions $2a = 11$ mm, $2b = 5.5$ mm

Experimental and numerical results on the study of the self-image in a rectangular copper waveguide of initial beams of THz radiation with a

field of the form (1.61), linearly polarized along the narrow wall of the waveguide, are given below. One can see from Table 1.6 that in the case of excitation of the waveguide by such a radiation, the signal spectrum at the waveguide input contains only waveguide modes with odd indices m and even indices n .

Unlike other types of excitations (see Section 1.1.1), additional equiphase cross sections of beam reconstruction are situated at the shortest distance from the input end of the waveguide.

Table 1.6

Relative fractions of energies U in the radiation spectrum of basic waveguide TE and TM modes for different values of mode indices for a beam of radius $w = 0.37$ polarized linearly along the narrow wall of the waveguide

| | $m \backslash n$ | 0 | 1 | 2 | 3 | 4 | 5 | 6 |
|-------------------|------------------|---|-------|---|-------|---|------|---|
| | 0 | – | 71.19 | 0 | 14.66 | 0 | 0.63 | 0 |
| $U_{mn}^{TE}, \%$ | 1 | 0 | 0 | 0 | 0 | 0 | 0 | 0 |
| | 2 | 0 | 0.65 | 0 | 0.82 | 0 | 0.06 | 0 |
| | 3 | 0 | 0 | 0 | 0 | 0 | 0 | 0 |
| | 1 | – | 0 | 0 | 0 | 0 | 0 | 0 |
| $U_{mn}^{TM}, \%$ | 2 | – | 10.40 | 0 | 1.46 | 0 | 0.04 | 0 |
| | 3 | – | 0 | 0 | 0 | 0 | 0 | 0 |

Experiments were made on the basis of a rectangular copper waveguide of dimensions $11 \times 55 \text{ mm}^2$ with an integer ratio a/b of its sides. The length $L = 287 \text{ mm}$ ($s' \approx 1.03$) of the waveguide reconstruction cross section for the given radiation beam ($s = 1.0$) and was refined in calculations by using the spectral technique described above. Figure 1.21 shows the calculated (1, 3, 4) and experimental (2, 5, 6) relative transverse field intensity distributions at the input (1, 2) and output (3–6) of the waveguide for initial radiation beams with relative waist radii $w = 0.27; 0.32; 0.37$. The nonzero field at the broad wall of the waveguide in the reconstruction cross section is explained in the calculations to the presence of the field of the corresponding waveguide modes at this wall [51], which synthesise the input radiation beam.

CHAPTER 1

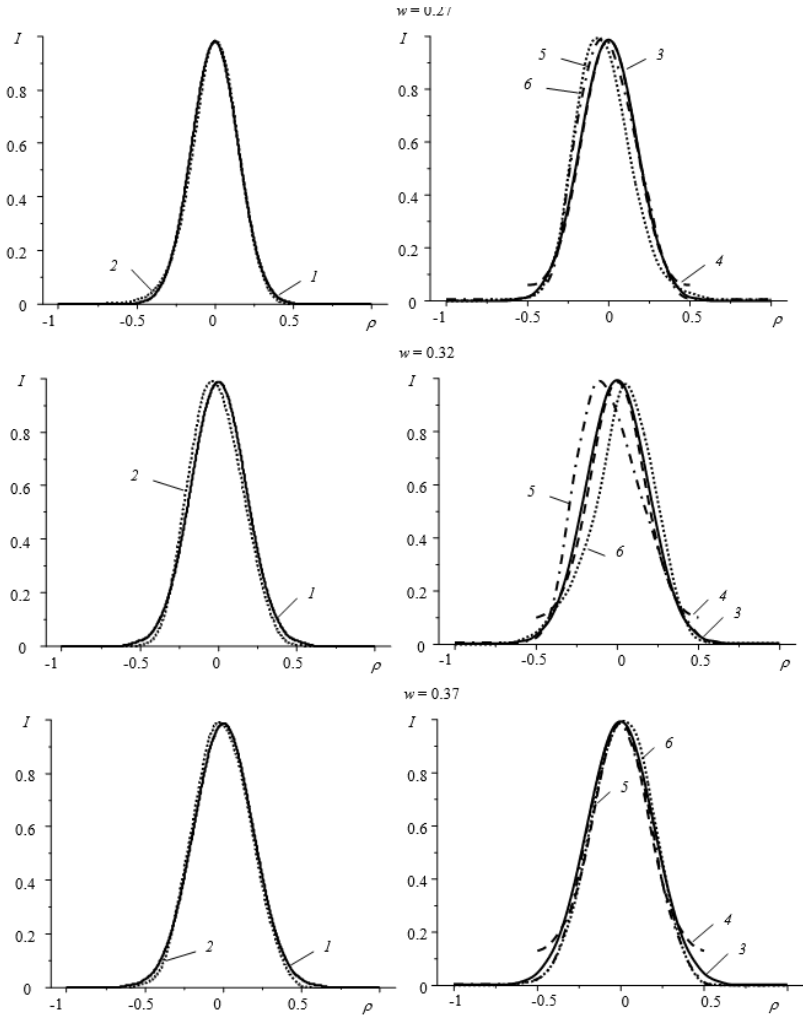


Figure 1.21. Theoretical [curves (1, 3, 4)] and experimental [curves (2, 5, 6)] relative transverse distributions of field intensity at the input [curves (1, 2)] and output [curves (3 – 6)] of the waveguide [curves (1, 2, 3, 6) correspond to distributions along the broad wall and curves (4) and (5) to distributions along the narrow wall of the waveguide for $w = 0.37$, $\rho = x/a$]

The reconstruction errors in the theoretical and experimental relative input distributions of the field intensity shown in Figure 1.21 were calculated from the expressions [77]

$$\delta_x = \sqrt{\int_{-a}^a [I_e(x, 0, L) - I_t(x, 0, L)]^2 dx},$$
$$\delta_y = \sqrt{\int_{-b}^b [I_e(0, y, L) - I_t(0, y, L)]^2 dy},$$

where I_e, I_t are respectively the experimental and theoretical relative distributions of the field intensity in the reconstruction cross section. The reconstruction of the input field is observed with sufficiently small errors. For example, for an initial wave beam with a waist radius $w = 0.37$, the reconstruction of its shape occurs with errors $\delta_x = 0.35\%$ and $\delta_y = 0.47\%$.